

Evaluation of Hybrid Micropile A-Frame-Geosynthetic-Reinforced Wall with Steel Guardrail Barrier for MASH Loading



APPLIED RESEARCH &
INNOVATION BRANCH

Ronald Y. S. Pak

Zhichao Zhang



COLORADO
Department of Transportation

The contents of this report reflect the views of the author(s), who is(are) responsible for the facts and accuracy of the data presented herein. The contents do not necessarily reflect the official views of the Colorado Department of Transportation or the Federal Highway Administration. This report does not constitute a standard, specification, or regulation.

Technical Report Documentation Page

1. Report No. CDOT-2021-11	2. Government Accession No.	3. Recipient's Catalog No.	
4. Title and Subtitle Evaluation of Hybrid Micropile A-Frame-Geosynthetic-Reinforced Wall with Steel Guardrail Barrier for MASH Loading		5. Report Date December 2021	
		6. Performing Organization Code	
7. Author(s) Ronald Y.S. Pak and Zhichao Zhang		8. Performing Organization Report No.	
9. Performing Organization Name and Address Department of Civil, Environmental & Architectural Engineering, University of Colorado Boulder, CO 80309-0428		10. Work Unit No. (TRAIS)	
		11. Contract or Grant No. R.218-02	
12. Sponsoring Agency Name and Address Colorado Department of Transportation - Research 2829 W Howard Pl, Denver CO 80204		13. Type of Report and Period Covered Final	
		14. Sponsoring Agency Code	
15. Supplementary Notes Prepared in cooperation with the US Department of Transportation, Federal Highway Administration			
16. Abstract This report presents the result of the evaluation of the adequacy and ability of a hybrid geosynthetic reinforced retaining wall in a truncated configuration for steep terrains to support steel bridge guardrails under the American Association of State Highway and Transportation Officials (AASHTO) Manual for Assessing Safety Hardware (MASH)'s Test-Level 4 impact loading. Intended to provide an engineering option particularly for marginal site or slope conditions, the hybrid design involves the installation of multiple pairs of vertical and inclined micropiles in the form of a structural A-frame through the backfill of a highway GRS wall into the foundation base, with a level of embedment that can strengthen the stability of both the wall and the slope. To determine the wall's ability to resist the more severe level of impact load-transfer from the roadside guardrail expected from MASH, use was made of the finite deformation and nonlinear modeling capability of finite element code LS-DYNA for the assessment. Using a combination of elastoplastic constitutive material models, a computer simulation platform was developed for modeling the hybrid soil-micropile-geofabric-guardrail design. To achieve a realistic representation of collision impact conditions pursuant to MASH on guardrails, compact modules of the finite element models originally developed by National Crash Analysis Center (NCAC) for a passenger car and single-unit truck vehicles were employed and integrated into the finite element W-beam and thriebeam guardrail-micropile-reinforced soil-wall analysis. From the analysis, the hybrid micropile-truncated GRS wall design was found to be capable of supporting the guardrail system under MASH TL-4 collision impact condition and a lateral design impact load of 88 kips for a 40" guardrail was recommended. Parallel to the computational synthesis, a laboratory scaled-model study was conducted to ascertain possible preferences of the geotextile type and soil condition for effective micropile installation, analytical-physical correlation and improving the construction procedure. The possibility of an equivalent-frontal collision impact condition to facilitate design iterations for MASH was also explored.			
17. Keywords geosynthetic reinforced soil (GRS), mechanically stabilized earth (MSE), micropiles, MASH TL-4, roadside guardrail, thriebeam, W-beam, finite element, LS-DYNA		18. Distribution Statement This document is available on CDOT's website http://www.coloradodot.info/programs/research	
19. Security Classif. (of this report) Unclassified	20. Security Classif. (of this page) Unclassified	21. No. of Pages	22. Price

ACKNOWLEDGEMENTS

The authors like to thank CDOT's DTD Applied Research and Innovation Branch for funding and support of this study. The Study Panel includes Trever Wang, Thien Tran, David Reeves, Aziz Khan (late), Andrew Pott, Steve Yip, Ryan Sullivan-Hope and Hoang Bui. Their input and suggestions during the project are gratefully acknowledged. The assistance of Scott Cusack, senior staff member of the structural and geotechnical engineering laboratory in the Department of Civil, Environmental & Architectural Engineering at CU Boulder is greatly appreciated.

EXECUTIVE SUMMARY

This report presents the result of the evaluation of the adequacy and ability of a hybrid geosynthetic reinforced retaining wall in a truncated configuration for steep terrains to support steel bridge guardrails under the latest American Association of State Highway and Transportation Officials (AASHTO) Manual for Assessing Safety Hardware (MASH)'s Test-Level 4 impact loading. Intended to provide an engineering option particularly for marginal site or slope conditions, the hybrid design involves the installation of multiple pairs of vertical and inclined micropiles in the form of a structural A-frame through the backfill of a highway GRS wall into the foundation base, with a level of embedment that can strengthen the stability of both the wall and the slope. To determine the wall's ability to resist the more severe level of impact load-transfer from the roadside guardrail expected from MASH, the study employed the finite deformation and nonlinear modeling capability of the finite element code LS-DYNA for the assessment. With the elastoplastic constitutive material models that have been calibrated and used in past NCHRP and CDOT projects, a computer simulation platform was developed for modeling the hybrid soil-micropile-geofabric-guardrail interactive load-transfer problem. To achieve a realistic representation of collision impact conditions pursuant to MASH on guardrails, compact modules of the finite element models originally developed by National Crash Analysis Center (NCAC) for a passenger car and single-unit truck vehicles were employed and integrated into the finite element guardrail-micropile-reinforced soil-wall analysis. From the analysis, the hybrid micropile-truncated GRS wall design was found to be capable of supporting the guardrail system under MASH TL-4 collision impact condition and a lateral design impact load of 88 kips for a 40" guardrail was recommended. Parallel to the computational synthesis, a laboratory scaled-model study was conducted to ascertain possible preferences of the geotextile type and soil condition for effective micropile installation, analytical-physical correlation and improving the construction procedure. The possibility of an equivalent-frontal collision impact condition to facilitate design iterations for MASH was also explored.

Table of Contents

1	INTRODUCTION	1
2	OBJECTIVES	4
3	APPROACH OF STUDY.....	4
4	FINITE ELEMENT MODELING OF MICROPILE-TRUNCATED GRS WALL WITH GUARD RAIL UNDER TL-4 COLLISION	5
4.1	Material Models for Soils, Geofabric, Micropiles, Concrete, Guardrail, Mounting Post and Interface Conditions for Hybrid Wall-Guardrail Design.....	5
4.2	Geometric Layout of Finite Element Model of Wall System for MASH-level Collision Assessment	14
4.3	Modeling of Vehicular Collisions	17
4.4	Experimental Insights on Drilling through Geosynthetic-Reinforced Soils.....	19
4.5	Setup of Initial Geostatic and Dynamic Load conditions	22
5	SIMULATION RESULTS AND ANALYSIS	23
5.1	Performance Checks of Vehicle-Guardrail-Micropile-GRS Wall Model in Collision Simulations.....	24
5.2	Vehicular Collision Loads on 40” Steel Guardrails on Hybrid Micropile-GRS wall	30
5.2.1	Oblique Passenger Car Impact	30
5.2.2	Oblique Single-Unit Truck Impact.....	32
5.2.3	Equivalent-Frontal Single-Unit Truck Impact	35
5.2.4	Soil Deformation in Hybrid GRS backfill from TL-4 Truck Impact.....	37
5.3	Displacement of Hybrid Wall and Foundation from Impact	39
6	IMPLEMENTATION OF RESEARCH TO ENGINEERING PRACTICE	41
7	CONCLUSIONS AND RECOMMENDATIONS	44
8	REFERENCES.....	46

LIST OF FIGURES

Figure 1.1: Road construction in steep slope and micropile installation equipment.....	2
Figure 1.2: CDOT worksheet B_504 for micropile A-frame truncated GRS wall design.....	3
Figure 4.1: Yield surface definition in Geologic Cap model	6
Figure 4.2: Mohr-Coulomb irregular hexagon envelope and classical experimental soil data on deviatoric plane in principal stress space [7]	8
Figure 4.3: Choices of approximation of Mohr-Coulomb irregular hexagon by Geological Cap or Drucker-Prager circular limit on the deviatoric plane	9
Figure 4.4: Cross-sectional geometries and arrangement of W-beam and thriebeam guardrails	12
Figure 4.5: Finite element models for a 6m-tall micropile A-frame truncated GRS walls.....	15
Figure 4.6: Finite element discretizations for micropile A-frame, guardrail, posts and grade beam	15
Figure 4.7: A 30m span of steel guardrail on micropile A-frame truncated GRS walls.....	16
Figure 4.8: NCHRP 350-based dynamic load specification.....	18
Figure 4.9: Finite element model of Geo Metro [16]	18
Figure 4.10: Finite element model of Ford F-800 truck [18]	19
Figure 4.11: Geosynthetics in experimental GRS drilling study: (a) a mesh geofabric and (b) a woven geofabric (Amoco 2044).....	21
Figure 4.12: Drilled-through geo-meshes in geosynthetic-reinforced sand	21
Figure 4.13: Drilled-through woven geofabrics (AMOCO 2044) in geosynthetic-reinforced sand.....	22
Figure 5.1: Computer models of vehicular collisions with guardrails	23
Figure 5.2: Sequential snapshots of F-800 truck colliding @ 90 km/hr and 15° oblique impact	25
Figure 5.3: Sequential snapshots of F-800 truck colliding @90 km/h & 15° with 0.91m (36”) thriebeam guardrail on micropile-truncated GRS wall	27
Figure 5.4: Sequential snapshots of F-800 truck colliding @80 km/h & 15° with 0.91m (36”) thriebeam guardrail on micropile-truncated GRS wall	29
Figure 5.5: Passenger car colliding with thriebeam guardrail on micropile-GRS wall	31
Figure 5.6: Top lateral displacement time history of 36” (0.91m)-high thriebeam beam guardrail under 25°oblique 100km/hr car impact: Peak $\delta_h = 0.31\text{m}$	32
Figure 5.7: Resultant impact force F_h time history from 25°oblique 100kmh car impact on 36” (0.91m) high thriebeam guardrail: Peak thrust=230 kN (52 kips)	32
Figure 5.8: Single unit truck running into 40” (1.01m)-high thriebeam guardrail on micropile-MSE wall at 90 kmh and15° angle.....	33
Figure 5.9: Top and bottom guardrail post displacements from 90 kmh -15°oblique truck collision on 40” thriebeam-pile-GRS wall	34
Figure 5.10: Resultant impact force F_h time history from 90 kmh -15° oblique truck collision on 40” thriebeam-pile-GRS wall: Peak thrust =390kN (88 kips)	34
Figure 5.11: Single unit truck running into 40”(1.01m) high thriebeam guardrail on micropile-GRS wall under 90° equivalent-frontal impact	35
Figure 5.12: Top and bottom 40” guardrail post displacements from 90kmh*sin(15°) equivalent-frontal truck collision on 40” thriebeam-pile-GRS wall	36
Figure 5.13: Resultant impact force F_h time history from 90kmh*sin(15°) equivalent-frontal truck collision on 40” thriebeam-pile-GRS wall: Max=425kN (96 kips)	36
Figure 5.14: Effective strain variation under in-situ geostatic condition:	37

Figure 5.15: Effective strain variation from effective frontal truck impact load38
Figure 5.16: Residual effective strain variation from effective frontal truck impact load:.....38
Figure 5.17: Simplified impact load time histories for hybrid micropile-GRS wall assessment
and design.....40
Figure 5.18: Barrier lateral displacement under different frontal impact load levels [6].....40
Figure 5.19: Lateral displacement of front wall panel by different impact force levels:40
Figure 6.1: CDOT Worksheet_B-504-A342
Figure 6.2: CDOT Worksheet_B-504-A542
Figure 6.3: CDOT Worksheet_B-504-V243

LIST OF TABLES

Table 1.1: Evaluation criteria for MASH TL-4 Longitudinal Barriers.....	3
Table 1.2: Vehicle weights and speeds of NCHRP-350 versus MASH TL-4 for TL-4 [15]	4
Table 4.1: Relationship between the friction angle φ and θ for.....	10
Table 4.2: Geological Cap Parameters for backfill soil in GRS region for $\varphi=34^\circ$ at $b=0.5$	10
Table 4.3: Geological Cap parameters for soil with $\varphi=40^\circ$ at $b=0.5$	10
Table 4.4: Parameters for geotextile kinematic-plastic material model	11
Table 4.5: Parameters for concrete by linearly elastic model.....	11
Table 4.6: Parameters for steel dowel and rebar for bilinear kinematic-plastic model	12
Table 4.7: Steel guardrail and post parameters	13
Table 4.8: Interfacial friction coefficients between materials	14

1 INTRODUCTION

For road constructions in mountainous areas with undulating terrain, complex geological setting and steep slopes, deep cuts and fills are often necessary to provide an acceptable subgrade for efficient traffic flows. Because of the continuous increase in population and interstate commerce nowadays, many highways are or will be in need of expansion, may it be totally new construction or adding lanes on one side of existing roads. The topography of the mountainous areas is generally characterized by river or valley on one side and cliff or steep slope on the other side, with insufficient room for conventional construction and heavy equipment as illustrated in Figure 1.1. In the Rocky Mountain region, the increasing frequency of having to deal with marginal slope stability problems, especially under the increasingly extreme weather and erosion conditions, has further aggravated the challenge in its infrastructure plan and road improvement projects. As one of its efforts to help tackle the construction demand and difficulties, CDOT developed a hybrid retaining wall design for such challenging conditions by integrating the use of micropiles, roadside barrier and geosynthetic-reinforced soil (GRS) as an engineering option (see Figure 1.2 and [6]) that can provide sufficient the foundation and anchorage support necessary for test level 4 (TL-4) impact loads on roadside barriers according to NCHRP-350's standards [1] despite the more limited truncated-GRS wall configurations. The central idea was to make use of a pair of vertical and inclined micropiles that are connected as an A-frame and install them through a geosynthetic-reinforced soil backfill of the wall. With sufficient additional micropile penetration and grouting into the foundation slope, the design allows not only a reduction of the amount of excavation that can be risky for unfavorable slope conditions but also raise the long-term factor of safety of the marginal slope itself. These potential benefits of the hybrid wall design were evaluated and demonstrated in [6]. Recognizing that car and trucks have become generally heavier and more powerful since NCHRP Report 350, however, the latest American Association of State Highway and Transportation Officials (AASHTO)'s Manual for Assessing Safety Hardware (MASH) [25] has posted more stringent minimum conditions on structural adequacy and occupancy risk in the form of criteria A, D, F, H, and L which must be satisfied in a timely schedule (see Table 1.1 and Table 1.2). With the stipulation that the final approval of any proposed roadside safety hardware be conditioned on satisfactory full-scale crash tests as well as advanced finite element modeling, a

careful re-assessment and possible upgrade of current guardrail barriers and the adequacy of their foundation support is thus mandatory.



Figure 1.1: Road construction in steep slope and micropile installation equipment

By the updated criteria in MASH, the change in TL-4 is significantly higher than NCHRP-350's standards, relative to other TL levels (see, e.g., [13]). For the passenger car case as an example, the weight of the vehicle for TL-4 has increased from 1800 lb (820 kg) to 2400 lb (1100 kg), the speed from 56 mph (90 kmh) to 62 mph (100 kmh), and the impact angle from 20° to 25°. For single-unit trucks (SUT), while the impact angle stays at 15°, the weight has increased from 17600 lb (8000 kg) to 22,000 lb (10000 kg) and the speed raised from 50 mph (80 kmh) to 56 mph (90 kmh). In terms of the Impact Severity Index which is calculated as the normal component of the vehicle's linear momentum with respect to the barrier, the increase in TL-4 is about 56% by MASH. With the focus on steel roadside guardrails, the goal of this project is to provide an engineering evaluation of the adequacy of the hybrid micropile A-frame truncated GRS wall design with respect to TL-4 conditions and check if any modification is necessary to handle the more demanding impact/collision condition.

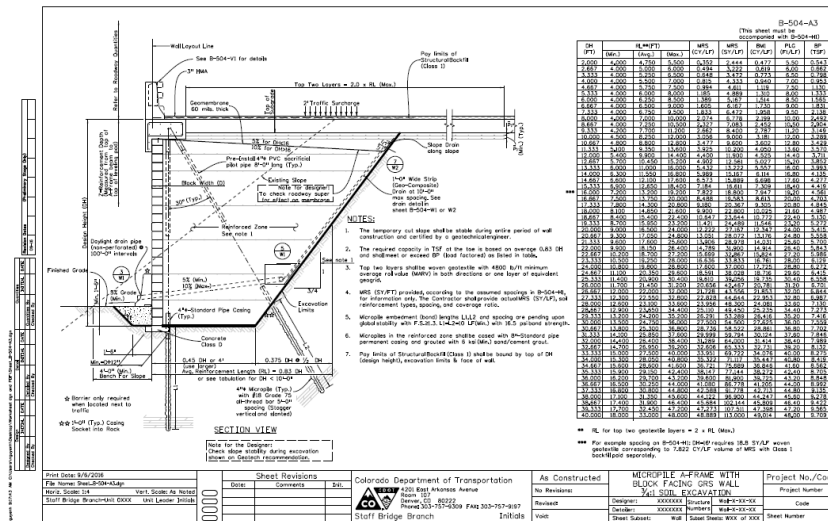


Figure 1.2: CDOT worksheet B_504 for micropile A-frame truncated GRS wall design

Evaluation Factors	Evaluation Criteria	MASH Test
Structural Adequacy	<i>A. Test article should contain and redirect the vehicle or bring the vehicle to a controlled stop; the vehicle should not penetrate, underide, or override the installation although controlled lateral deflection of the test article is acceptable.</i>	10, 11, 12
Occupant Risk	<i>D. Detached elements, fragments, or other debris from the test article should not penetrate or show potential for penetrating the occupant compartment, or present undue hazard to other traffic, pedestrians, or personnel in a work zone. Deformations of, or intrusions into, the occupant compartment should not exceed limits set forth in Section 5.2.2 and Appendix E of MASH.</i>	10, 11, 12
	<i>F. The vehicle should remain upright during and after collision. The maximum roll and pitch angles are not to exceed 75 degrees.</i>	10, 11
	<i>G. It is preferable, although not essential, that the vehicle remain upright during and after the collision.</i>	12
	<i>H. Occupant ridedown velocities (OIV) should satisfy the following limits: Preferred value of 30 ft/s, or maximum allowable value of 40 ft/s.</i>	10, 11
	<i>I. The occupant ridedown accelerations should satisfy the following: Preferred value of 15.0 g, or maximum allowable value of 20.49 g.</i>	10, 11

Table 1.1: Evaluation criteria for MASH TL-4 Longitudinal Barriers

NCHRP 350 vs. MASH Vehicles





Vehicle Class	NCHRP 350	MASH
Small car 	820C Weight: 1,809 lb	1100C Weight: 2,420 lb
Pickup Truck 	2000P Weight: 4,409 lb	2270P Weight: 5,000 lb
Single Unit Truck 	8000S Weight: 17,636 lb	10000S Weight: 22,000 lb
Tractor Trailer 	36000V Weight: 79,366 lb	36000V Weight: 79,300 lb

Table 1.2: Vehicle weights and speeds of NCHRP-350 versus MASH TL-4 for TL-4 [15]

2 OBJECTIVES

This research sought to evaluate the performance of the hybrid micropile A-frame-truncated GRS wall design with steel bridge rails under MASH’s test level 4 impact conditions. Aimed to develop an analytical framework and deeper engineering insight on the nature of the resulting vehicle-guardrail-post-foundation interaction and the resultant effective impact load time histories for design, this report describes the dynamic analysis and simulation method that employed elastoplastic finite element modeling of not only the soil, concrete, micropile, guardrails but also the car and truck in the evaluation of the wall’s sufficiency under the more severe condition. A comparison and correlation of the results from the collision analysis for MASH’s standard to the wall’s past evaluation on the basis of NCHRP 350 was also of interest.

3 APPROACH OF STUDY

With the number of different material components (e.g., soil, geosynthetics, concrete, steel) in a composite system as in a truncated GRS mass with micropiles, guardrails and grade beam bearing on a natural slope, the use of elementary soil mechanics methods for the analysis and design of a hybrid wall system is clearly unreliable for the proposed assessment. Owing to its ability to handle

large deformation and model soil and structural materials near or at failure as expected under MASH conditions, the versatile elastoplastic nonlinear finite element code LS-DYNA was adopted (see [8, 11]). To provide a realistic assessment of the design's behavior as well as their mechanical interaction with each other in the time frame of the project, the constitutive model modules and material parameters used in [6] were chosen to facilitate a gain in efficiency in synthesis and interpretations.

4 FINITE ELEMENT MODELING OF MICROPILE-TRUNCATED GRS WALL WITH GUARD RAIL UNDER TL-4 COLLISION

To ensure realistic finite element modeling of physical structures, a critical first step is the choice of material and interface models, meshing and their overall layouts. In this study, the system includes the soil, geofabric, micropiles, concrete, steel, guardrail, support post and vehicle models for the collision load-transfer modeling. To enable appropriate interpretation of the research results, a brief description of the choice and modeling of each aspect is given in the following sections:

4.1 Material Models for Soils, Geofabric, Micropiles, Concrete, Guardrail, Mounting Post and Interface Conditions for Hybrid Wall-Guardrail Design

(a) Soil:

Soil is the weakest but also the major component of the hybrid GRS-micropile design and the foundation system. To allow for its possible failure and large deformation, the elastoplastic 3D Geologic Cap model (DiMaggio and Sandler [9], Hallquist [10]) as MAT 25 in LS-DYNA was adopted for the soil medium. The details of the module can be found in LS-DYNA's user's manual [8]. As a generalization of Drucker-Prager model, the key capability of the Geological Cap (GC) model has over the classical Mohr-Coulomb model in soil mechanics is not only that it does not have the latter's corners which often creates numerical problems, but also its added ability to model plastic volumetric compaction via a movable cap on the conical yield surface. In the model, purely volumetric response is elastic until the stress point hits the cap surface, beyond which the rate of plastic volumetric strain is controlled by the hardening law. The plastic yield surface of the model consists of three regions: a shear failure envelope $f_1(\boldsymbol{\sigma})$, an elliptical cap $f_2(\boldsymbol{\sigma}, \kappa)$, and a tension cutoff region $f_3(\boldsymbol{\sigma})$, where $\boldsymbol{\sigma}$ is the soil's stress tensor and κ is a hardening parameter.

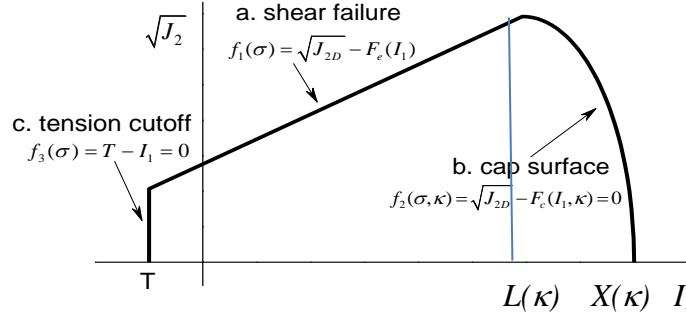


Figure 4.1: Yield surface definition in Geologic Cap model

The functional forms of the three surfaces are:

- a. For shear failure region where $T \leq I_1 < L(\kappa)$:

$$f_1(\sigma) = \sqrt{J_2} - F_e(I_1) = 0 \quad (1)$$

- b. For elliptical cap region where $L(\kappa) \leq I_1 < X(\kappa)$:

$$f_2(\sigma, \kappa) = \sqrt{J_2} - F_c(I_1, \kappa) = 0 \quad (2)$$

- c. For tension cutoff region where $I_1 = T$:

$$f_3(\sigma) = T - I_1 = 0 \quad (3)$$

where I_1 is the first invariant of the stress tensor and J_2 is the second invariant of the deviator stress tensor, and T is the tension cutoff value. $F_e(I_1)$ in Eq. (1) is defined in LS-DYNA as

$$F_e(I_1) = \alpha - \gamma e^{-\beta I_1} + \theta I_1 \quad (4)$$

With γ and β set to zero in this study, Eq. (4) is reduced to

$$F_e(I_1) = \theta * I_1 + \alpha \quad (5)$$

Eq. (5) is identical to the Drucker-Prager failure criterion [10] and the parameters α and θ are related to the classical Mohr-Coulomb's cohesion and friction angle parameters c and ϕ . The function $F_c(I_1, \kappa)$ in Eq. (2) is defined by

$$F_c(I_1, \kappa) = \frac{1}{R} \sqrt{[X(\kappa) - L(\kappa)]^2 - [I_1 - L(\kappa)]^2} \quad (6)$$

$$X(\kappa) = \kappa + R F_e(\kappa) \quad (7)$$

$$L(\kappa) = \begin{cases} \kappa & \text{if } \kappa > 0 \\ 0 & \text{if } \kappa \leq 0 \end{cases} \quad (8)$$

with R being a shape factor that represents the ratio of major to minor axes of the elliptical cap, $X(\kappa)$ denoting the intersection of the cap surface with the I_1 axis and κ being a hardening parameter. The latter is related to the plastic volume change ε_v^P through the hardening law

$$\varepsilon_v^P = W \{1 - e^{-D[X(\kappa) - X_0]}\} \quad (9)$$

where W characterizes the plastic volumetric strain's limit, D denotes the total volumetric plastic strain rate, and X_0 represents the initially-set intersection of the cap surface with the I_1 -axis in the stress space and defines the size of the initial elastic domain of the soil.

While the GC model has been used and calibrated in multiple DOTs or NCHRP projects, it should be noted that it has its limitations in regard to representing real soil behavior fully. As shown in Fig. 4.2, experimental soil test results are generally closer to the Mohr-Coulomb irregular hexagonal shape on the deviatoric π -plane in the 3D principal stress space (Scott [7]), i.e., there is a dependence of the shear strength on the ratio of the major, minor as well as the intermediate principal stresses $\sigma_1, \sigma_2, \sigma_3$, than the pure circular locus that is assumed in the Drucker-Prager and GC models. Upon knowing the eventual failure combination of $(\sigma_1, \sigma_2, \sigma_3)$ or its Lode's angle θ_{Lode} , on the other hand, the shear strength parameters c and φ of Mohr-Coulomb criterion can be chosen analytically to give the same failure stress state via the strength parameters α and θ of the Geological Cap model. To obtain realistic predictions of the soil, an appropriate matching criterion is crucial so that a representation of soil's strength via the GC model is not overly conservative nor unconservative by under- or over-estimating its shear strength in three-dimensional problems. For a stress path that has a specific Lode's angle θ_{Lode} which is related to the intermediate principal stress ratio $b = (\sigma_2 - \sigma_3) / (\sigma_1 - \sigma_3)$, the Mohr-Coulomb failure criterion can be expressed in terms of the stress invariants as

$$\frac{I_1}{3} \sin \varphi - \sqrt{J_2} (\cos \theta_{Lode} + \frac{1}{\sqrt{3}} \sin \theta_{Lode} \sin \varphi) + c \cos \varphi = 0 \quad (10)$$

or

$$\sqrt{J_2} = \frac{\sqrt{3} \sin \varphi}{3(\sqrt{3} \cos \theta_{Lode} + \sin \theta_{Lode} \sin \varphi)} * I_1 + \frac{\sqrt{3} \cos \varphi}{\sqrt{3} \cos \theta_{Lode} + \sin \theta_{Lode} \sin \varphi} * c \quad (11)$$

where

$$\theta_{Lode} = \frac{1}{3} \arcsin\left(-\frac{3\sqrt{3}}{2} \frac{J_3}{J_2^{3/2}}\right), \quad -\frac{\pi}{6} \leq \theta_{Lode} \leq \frac{\pi}{6}, \quad \tan \theta_{Lode} = \frac{2\sigma_2 - \sigma_1 - \sigma_3}{\sqrt{3}(\sigma_1 - \sigma_3)} = \frac{2b - 1}{\sqrt{3}} \quad (12)$$

and J_3 is the third deviatoric stress invariant. Setting Eq. (11) and Eq. (5) to be the same for a specific θ_{Lode} , the Geological Cap strength parameters can be related to Mohr–Coulomb strength parameters via

$$\alpha = \frac{\sqrt{3} \cos \varphi}{\sqrt{3} \cos \theta_{Lode} + \sin \theta_{Lode} \sin \varphi} * c \tag{13}$$

$$\theta = \frac{\sqrt{3} \sin \varphi}{3(\sqrt{3} \cos \theta_{Lode} + \sin \theta_{Lode} \sin \varphi)} \tag{14}$$

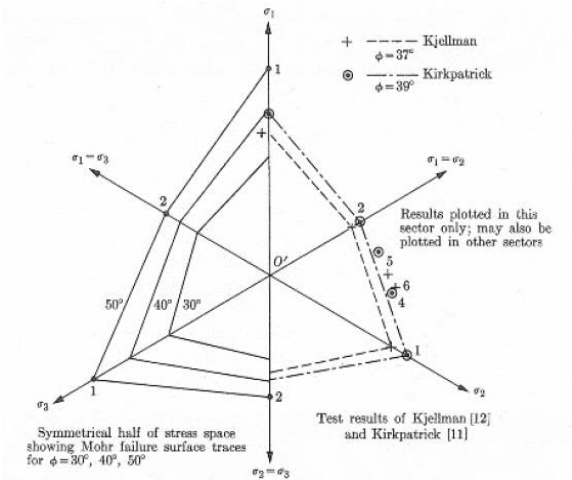


FIG. 7-8. View normal to deviatoric plane $\sigma_1 + \sigma_2 + \sigma_3 = C$, showing traces of Mohr-theory failure surface and test results.

Figure 4.2: Mohr-Coulomb irregular hexagon envelope and classical experimental soil data on deviatoric plane in principal stress space [7])

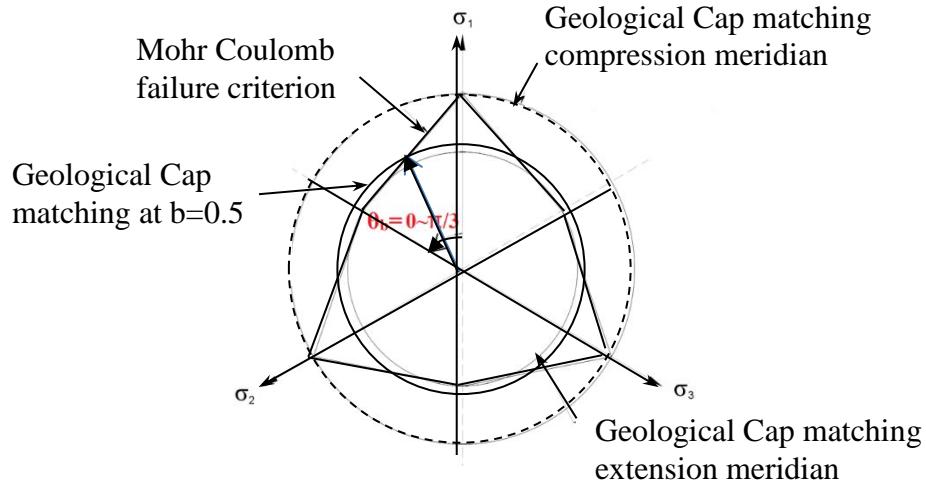


Figure 4.3: Choices of approximation of Mohr-Coulomb irregular hexagon by Geological Cap or Drucker-Prager circular limit on the deviatoric plane

Matching the Geological Cap model's strength with Mohr-Coulomb's in the conventional triaxial compression, ($\theta_{Lode} = -30^\circ$, $b=0$), for example, one finds

$$\alpha = \frac{6 \cos \varphi}{\sqrt{3}(3 - \sin \varphi)} * c \quad (15)$$

$$\theta = \frac{2 \sin \varphi}{\sqrt{3}(3 - \sin \varphi)} \quad (16)$$

To match their strengths in triaxial extension ($\theta_{Lode} = 30^\circ$, $b=1$), the relationship is

$$\alpha = \frac{6 \cos \varphi}{\sqrt{3}(3 + \sin \varphi)} * c \quad (17)$$

$$\theta = \frac{2 \sin \varphi}{\sqrt{3}(3 + \sin \varphi)} \quad (18)$$

As shown in Pak and Zhang [6], however, the stress state in the GRS soil region generally has an intermediate stress ratio b that averages to about 0.5 from the finite element solution (corresponding to $\theta_{Lode} = 0^\circ$) instead of 0 or 1 (see. Fig. 4.3). To be not overly conservative from using (15) and (16) nor un-conservative using (17) and (18), the Geological Cap model's strength parameter were taken to be

$$\alpha = c \cos \varphi \quad (19)$$

$$\theta = \sin \varphi / 3 \quad (20)$$

They correspond to matching the Geological cap model's failure surface with Mohr-Coulomb strength criterion at $b=0.5$. The resulting relationship between φ and θ are given in tabulated form in Table 4.1.

φ	29°	30°	31°	32°	33°	34°	35°	36°	37°	38°	39°	40°
θ	.1616	.1667	.1717	.1766	.1815	.1864	.1912	.1959	.2006	.2052	.2098	.2143

Table 4.1: Relationship between the friction angle φ and θ for intermediate stress ratio $b=0.5$

For the field condition of most interest in transportation practice, a sandy or gravelly soil with minimal cohesion and a friction angle of $\varphi=34^\circ$ and 40° were chosen as the nominal cases for the backfill and slope, with $\theta=0.186$ and $\theta=0.2143$, respectively. For these two cases, their complete set of chosen Geological Cap soil parameters for this study are given in Table 4.2 and 4.3 as in [6].

Parameter	K(MPa)	G(MPa)	α (kPa)	β (MPa-1)	γ (MPa)	θ_{GRS}
Value	16 to 48	7 to 22	2	0	0	0.1864
Parameter	W	D(MPa-1)	R	X_0 (kPa)	Tension Cutoff (MPa)	Soil density (kg/m ³)
Value	2.5	0.00725	4	from 20~400kPa	0	1596

Table 4.2: Geological Cap Parameters for backfill soil in GRS region for $\varphi=34^\circ$ at $b=0.5$

Parameter	K(MPa)	G(MPa)	α (kPa)	β (MPa-1)	γ (MPa)	θ_{slope}
Value	32.89	15.18	2.7	0	0	0.2143
Parameter	W	D(MPa-1)	R	X_0 (kPa)	Tension Cutoff (MPa)	Soil density (kg/m ³)
Value	2.5	0.00725	4	0	0	1596

Table 4.3: Geological Cap parameters for soil with $\varphi=40^\circ$ at $b=0.5$

(b) Geotextile:

To characterize the mechanical behavior of the geofabrics in the GRS, the bilinear kinematic-plastic model in LS-DYNA was adopted (see Fig. 4.5). Using Amoco 2044 (US4800) as a reference geotextile as in the previous CDOT project [6], the adopted material parameters for the geotextile with respect to the constitutive model are given in Table 4.4.

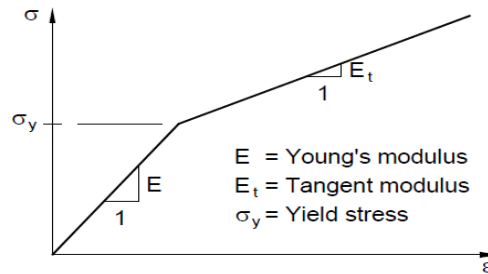


Figure 4.5: Stress-strain relationship of bilinear kinematic-plastic material model in LS-DYNA

Density (kg/m ³)	Yield stress σ_y (MPa)	Initial elastic modulus E (MPa)	Post-yield tangent modulus E_t (MPa)	Poisson's ratio ν
1000	4.33	433	0 or 162	0.3

Table 4.4: Parameters for geotextile kinematic-plastic material model

(c) Concrete:

Concrete elements of the system such as wall facing, grade beams and micropiles are modeled as a linear elastic material model with moduli given in Table 4.5.

Parameter	Density (kg/m ³)	Elastic modulus E (GPa)	Poisson ratio
Value	2320	25	0.15

Table 4.5: Parameters for concrete by linearly elastic model

(d) Steel reinforcements:

The steel elements in the wall such as dowels, rebars and anchors are assumed to be linearly elastic with the material parameters given in Table 4.6.

Parameters	Density (kg/m ³)	σ_y (MPa)	E(GPa)	E_t (GPa)
Values	7800	235	210	2

Table 4.6: Parameters for steel dowel and rebar for bilinear kinematic-plastic model

(e) Steel W-beam and thriebeam guardrails with support posts

The roadside hardware of interest in this study was steel guardrails under MASH's TL-4 conditions and how they affect the performance of the micropile- GRS wall. Given the great variety of steel guardrail sections that are available in the market (e.g., [23]), decision was made to focus on W-beam and thriebeam with nominal cross-sectional dimensions given in Fig. 4.4 with their equivalent material parameters given in Table 4.7. Both types of guardrails were taken to be connected through wood blocks to tubular steel posts with an outer diameter of 8" (20cm) and 0.5cm thickness.

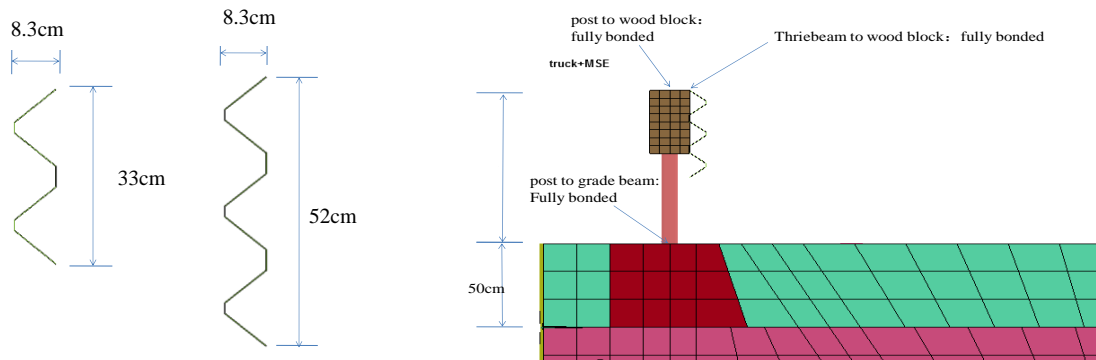


Figure 4.4: Cross-sectional geometries and arrangement of W-beam and thriebeam guardrails

Steel W-beam	density (kg/m ³)	σ_y (MPa)	E(GPa)	E_t (GPa)	thickness
	7800	385	210	0	5mm
	overall rail depth (m)			top height (m)	
	0.33			0.67, 0.91, 1.01	

Steel Thriebeam	density (kg/m ³)	σ_y (MPa)	E(GPa)	E_t (GPa)	thickness (mm)
	7800	385	210	0	5mm
	overall rail depth (m)			top height (m)	
	0.52			0.67, 0.91, 1.01	

Steel support posts	density (kg/m ³)	σ_y (MPa)	post spacing (m)	E & E_t (GPa)	dimensions
	7800	385	2m	210, 0	OD=0.2, ID=0.19 Thickness=0.005
	Anchorage (m)			height above grade (m)	wood block E(GPa)
	0.5 in grade beam			same as rail height	10

Table 4.7: Steel guardrail and post parameters

(f) Interfacial conditions between materials or components:

Concrete material in the hybrid wall includes micropile, grade beam and front wall panels. The contact conditions were taken to be either tied or frictional between different materials with parameters given in Table 4.8. Bonded contact was used between micropiles and grade beam because of the expected cementation of concrete. Assuming proper placement and compaction of the backfill on the foundation soil, bonded contact was adopted for the interface between the backfill and foundation soil.

guardrail post to grade beam	guardrail post to wood block	Wood block to guardrails	Veh to road, barrier surfaces	guardrail post to grade beam	guardrail post to wood block	Wood block to Thriebeam/W-beam	Veh to road barrier surfaces
bonded	bonded	bonded	0.45	bonded	bonded	bonded	0.45

GRS to fdn	piles to grade beam	piles to fdn	barrier to soil	wall to soil	geotextile to soil	geotextile to wall	wall toe to fdn
bonded	bonded	bonded	0.45	0.45	0.45	tied	free

Table 4.8: Interfacial friction coefficients between materials

4.2 Geometric Layout of Finite Element Model of Wall System for MASH-level Collision Assessment

To evaluate the adequacy of the micropile A-frame-truncated GRS wall to support steel guardrails for MASH conditions, the benchmark case of a 6m-tall 30m-long hybrid wall in a truncated shape with a periodic set of micropiles at 3m spacing on a 45° back-slope in [6] as shown in Figure 4.5 was employed. The GRS wall region was discretized into twelve soil layers with geotextile sheets in between. The backfill and slope regions were modeled by 8-node constant stress solid elements as did the micropiles and grade beam whose meshes are shown in Figure 4.6. They were all evaluated with one-point integration and viscous hourglass control in the nonlinear elastoplastic analysis. The geotextile sheets were set to be 2mm thick dimensionally and discretized using 4-node Belytschko-Tsay membrane elements for their minimal flexural stiffness (see <http://www.dynasupport.com/tutorial/ls-dyna-users-guide/elements>) while the steel bars were discretized as beam elements. The front concrete wall panel that covers the GRS front face was modeled by 4-node shell elements with a thickness of 10 cm. To ensure that the non-symmetrical response of the guardrail-post-foundation upon oblique vehicular collisions according to MASH condition is adequately captured, a finite element model of a 30 m long region of the truncated GRS wall with rail posts at 2 m spacing was employed in this study (see Figure 4.7).

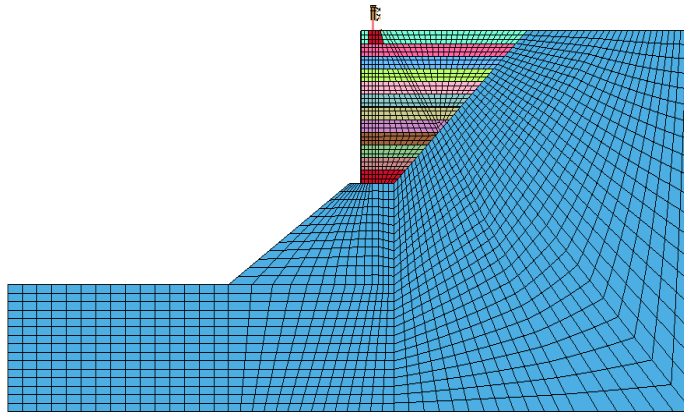


Figure 4.5: Finite element models for a 6m-tall micropile A-frame truncated GRS walls with steel guardrail as safety barriers

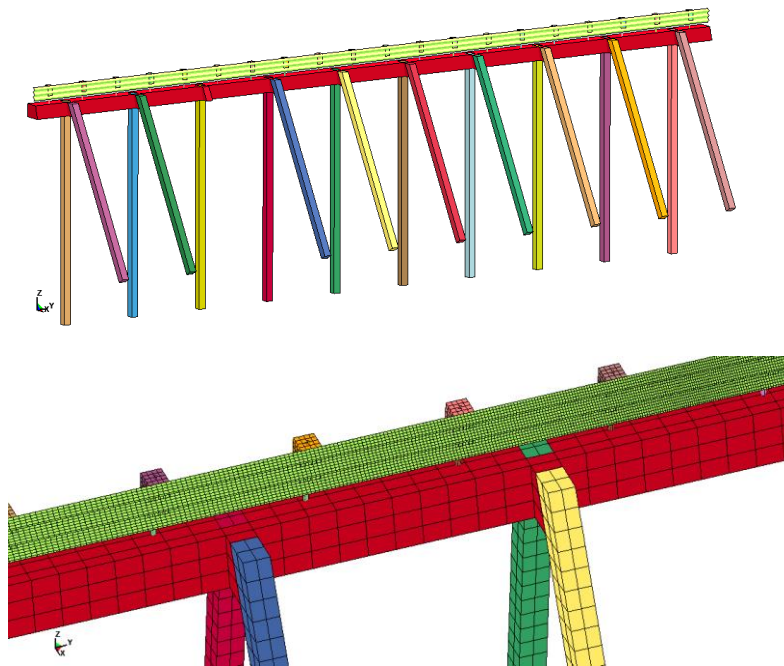


Figure 4.6: Finite element discretizations for micropile A-frame, guardrail, posts and grade beam

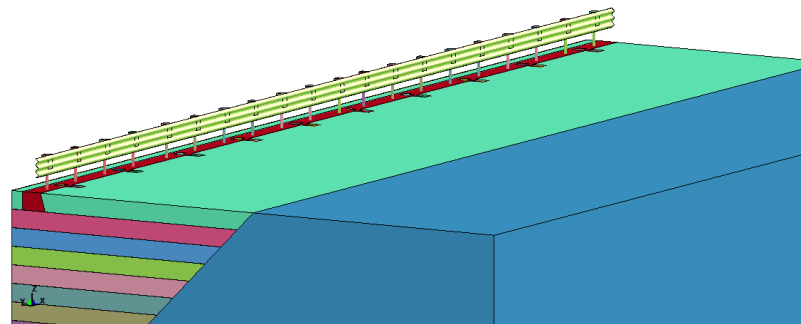
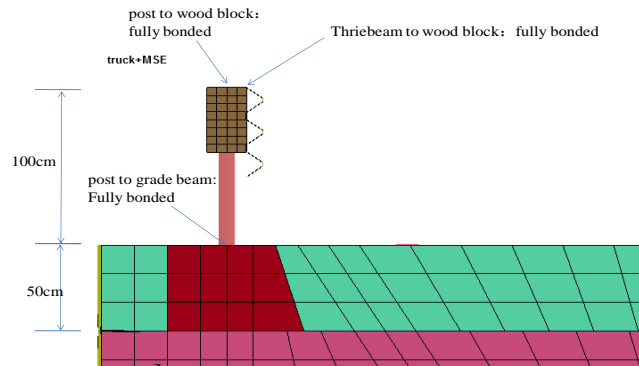


Figure 4.7: A 30m span of steel guardrail on micropile A-frame truncated GRS walls

Because of the high number of material components and interfaces in the hybrid GRS-pile-barrier-slope system, the effort in developing the 3D finite element model was significant even with material and connection simplifications wherever they were considered reasonable. For the micropiles, for example, an equivalent sectional stiffness approach was employed for their regions whose cross-sectional dimensions were taken to be a 27cm square but their Young's modulus could be adjusted to account for different physical sizes or reflect the degree of soil or geofabric disturbance as a result of the micropile field installation process where appropriate.

With the aforementioned choices of material parameters and finite element layout for the wall, the model for the hybrid A-frame micropile-GRS-guardrail-grade beam-wall system built on a sloping terrain in the benchmark configuration was assembled for testing its capacity to resist the higher collision impact under MASH. In summary, the key components of the hybrid wall model were

1. a truncated reinforced soil region with layers of soil and geotextiles and a front concrete facing,
2. multiple pairs of vertical and inclined micropiles that were aligned to meet each other at their pile caps at equally spaced vertical planes to form a set of A-frames along the length of the roadway,
3. the concrete micropiles were extended and penetrated into the back slope region with 2.5m embedment,
4. the W-beam or thriebeam guardrails were taken to be connected to the same set of support posts which were anchored to the grade beam that was connected to all the pile caps to form an integral soil-foundation-structure system.

4.3 Modeling of Vehicular Collisions

In the NCHRP Report 350-based approach, the vehicular impact on a barrier was allowed to be simplified to a pre-determined dynamic force time history (see Figure 4.8) without the requirement to account for vehicle-guardrail-foundation interaction effects. Such an approach has greatly reduced the complexity of the dynamic response analysis and design calculations. In MASH, however, a truer assessment of the collision process via a comprehensive finite element model of the full collision situation as well as a corresponding full-scale physical crash test for validation is required for final hardware approval. With the generally heavier weight, higher speed and larger impact angle of the incoming vehicle by MASH, more severe deformation and disintegration of both the car and barrier system are expected to be inevitable. While it is beyond the scope and resources of the study of the micropile-GRS wall to pursue such an approach fully, the incorporation of a higher-level modeling that can give a realistic account of the vehicle's interaction with the guardrail to characterize the elevated impact load transfer to the hybrid micropile-GRS wall would clearly be desirable. To this end, 2 computer aided engineering (CAE) finite element vehicle models developed for crash studies were found to be workable for the present project: a version of the 820kg Geo Metro as a passenger car and a version of the 10000kg Ford F-800 as a single-unit truck (see Figure 4.9 and Figure 4.10). While the Geo Metro model was suitable more for NCHRP Report 350 than MASH's passenger car condition, the Ford F-800 has been used in crash tests to check against the current MASH single unit-truck criteria (e.g., [16] and [18]). Both models are sophisticated finite element models that were originally developed by the National Crash Analysis Center (NCAC) [17]. With tens of thousands of degrees of freedom, they have detailed numerical

representations of the structural frame, bumpers, drive train, suspensions, wheels, tires, connections, steering subsystems as well as and many interior components. Constructed with solid, shell, beam and discrete elements, nonlinear material constitutive modules from elastoplastic to viscoelastic and contact options were incorporated in the computer models and calibrated by both laboratory material and crash tests (e.g., see [16]). To reduce the severe computational demand of the complex vehicle-guardrail-micropile-GRS-foundation interaction in the collision simulations, analytical reductions of the 3D multi-region finite element models were sought and employed where possible in the study so long as they did not compromise the key dynamic aspects of the vehicles and the collision event. The final renditions of the numerical Geo Metro and Ford F-800 models employed had the number of elements as 16268 and 40224, respectively.

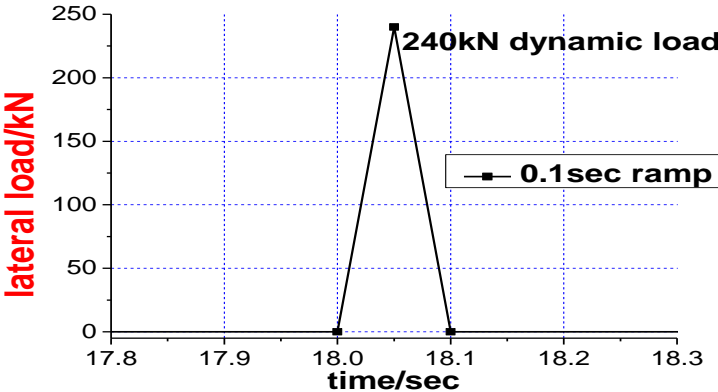


Figure 4.8: NCHRP 350-based dynamic load specification

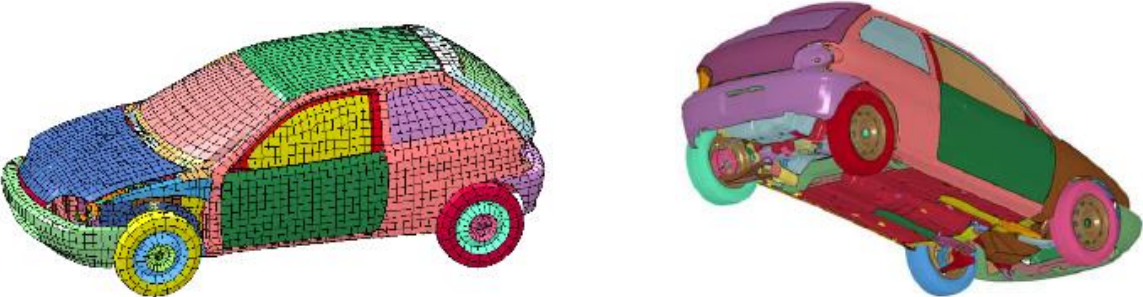


Figure 4.9: Finite element model of Geo Metro [16]

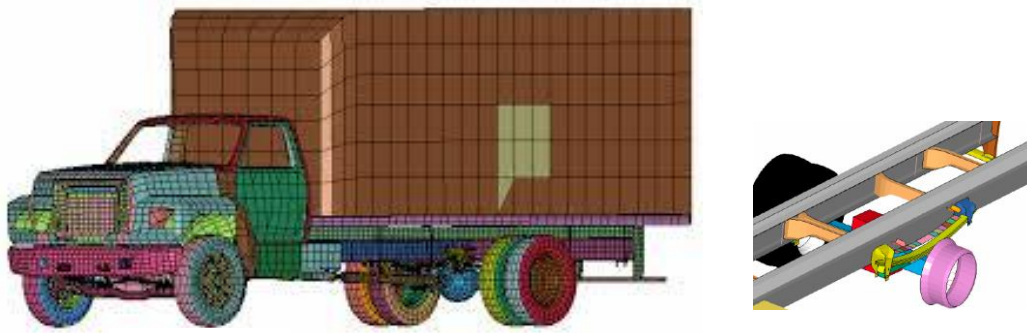


Figure 4.10: Finite element model of Ford F-800 truck [18]

4.4 Experimental Insights on Drilling through Geosynthetic-Reinforced Soils

For effective field implementation of the hybrid GRS wall design as well as to gage the appropriateness of the analytical representation of the installed micropile-geofabric condition in the finite element model, a laboratory-scale experimental study was conducted in CU's structural-geotechnical laboratory. Of particular interest is the degree of disturbance of the soil or the geosynthetic from the drilling process for the micropile installation and how it might be related to the geosynthetic's type as well as the soil condition. To provide some basic insights into these aspects, a series of laboratory drilling tests were performed on several compacted soil samples that were reinforced by two kinds of geofabrics (see Figure 4.11). In these tests, the soil used was a local medium coarse sand with a D_{50} of 0.75mm. It was compacted at 1.5" (3.8 cm) thick increments using a heavy 6" (15 cm) diameter flat-ended steel barrel to achieve a final soil height of 14" (36 cm) with single sheets of geofabric being laid at 10.5", 7" and 3.5" (27 cm, 18 cm and 9 cm) depths during specimen preparation. The dry density of the soil was around 99 lb/ft³ (1585kg/m³) which is very close to the value of 1596 kg/m³ that was specified for the finite element model of the backfill soil (see Table 4.2). The boring was achieved all the way down to the bottom of the soil using an electric drill at low speed with a 2.5" (6.35 cm) diameter drill cup that was attached to a steel extension rod. The test series included having the sand in (a) a dry state with the geo-mesh, (b) a moisten state at 10% water content with the geo-mesh and (c) a moisten condition at 10% water content with the woven geofabric. Upon completion of the drilling in each case, the soil was excavated manually with care to examine the condition of the geofabrics and the hole layer by layer. The key observations from the experimental program were as follows:

1. In the dry sand test, the top fabric layers at 3.5” depth were found to curl up upon drilling (see Figure 4.12), but the drilling through the second and third geofabric sheets at 7” and 10.5” depth had much less such problem.
2. In the case of the moist sand, the ease of drilling improved distinctly for both the geo-mesh and the woven geofabric, with no more curl-up problem in their top fabric layer. This can be attributed to the beneficial effects of matric suction or apparent cohesion [12] in a partially saturated soil which led to a higher overburden effective vertical stress, resulting in extra frictional resistance in the geofabric plane against boring actions.
3. Close inspection of the geo-mesh sheets and the woven geofabrics after the drill-through revealed some difference in their residual conditions. While both of the geotextiles around the borehole appeared to be intact, the mesh/grid-type geofabrics suffered from having a strand or 2 being pulled out from them as a result of the boring action (see Figure 4.12). In contrast, the woven geosynthetic did not show much sign of such problems (see Figure 4.13). The distinction in response between the 2 geofabrics to coring likely stems from the stronger but more spatially discrete nature of the material resistance in the former and the more uniform and continuous distribution of the fabric resistance in the latter.

While the generality and practical relevance of these observations need to be confirmed in full scale field conditions, the experimental program suggests that (a) the weight from a modest depth of overburden soil on a geofabric layer is sufficient to hold the geofabric planar during the drilling, (b) the effective extra vertical stress provided by the matric suction in a partially saturated soil (not an uncommon soil condition in field compaction practice) is helpful in holding down the fabric under drilling actions, (c) a woven geofabric like Amoco 2044 would be more suitable for the hybrid micropile-GRS wall design than a mesh- or grid-type geosynthetic for the GRS construction, and (d) the assumed contact condition between the micropiles and the geosynthetic-reinforced soil with woven fabrics in the adopted LS-DYNA finite element model was reasonable with respect to the experimental results.

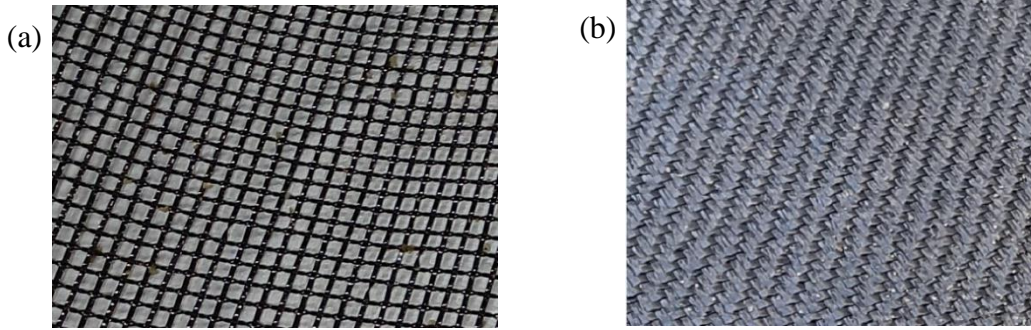


Figure 4.11: Geosynthetics in experimental GRS drilling study: (a) a mesh geofabric and (b) a woven geofabric (Amoco 2044)

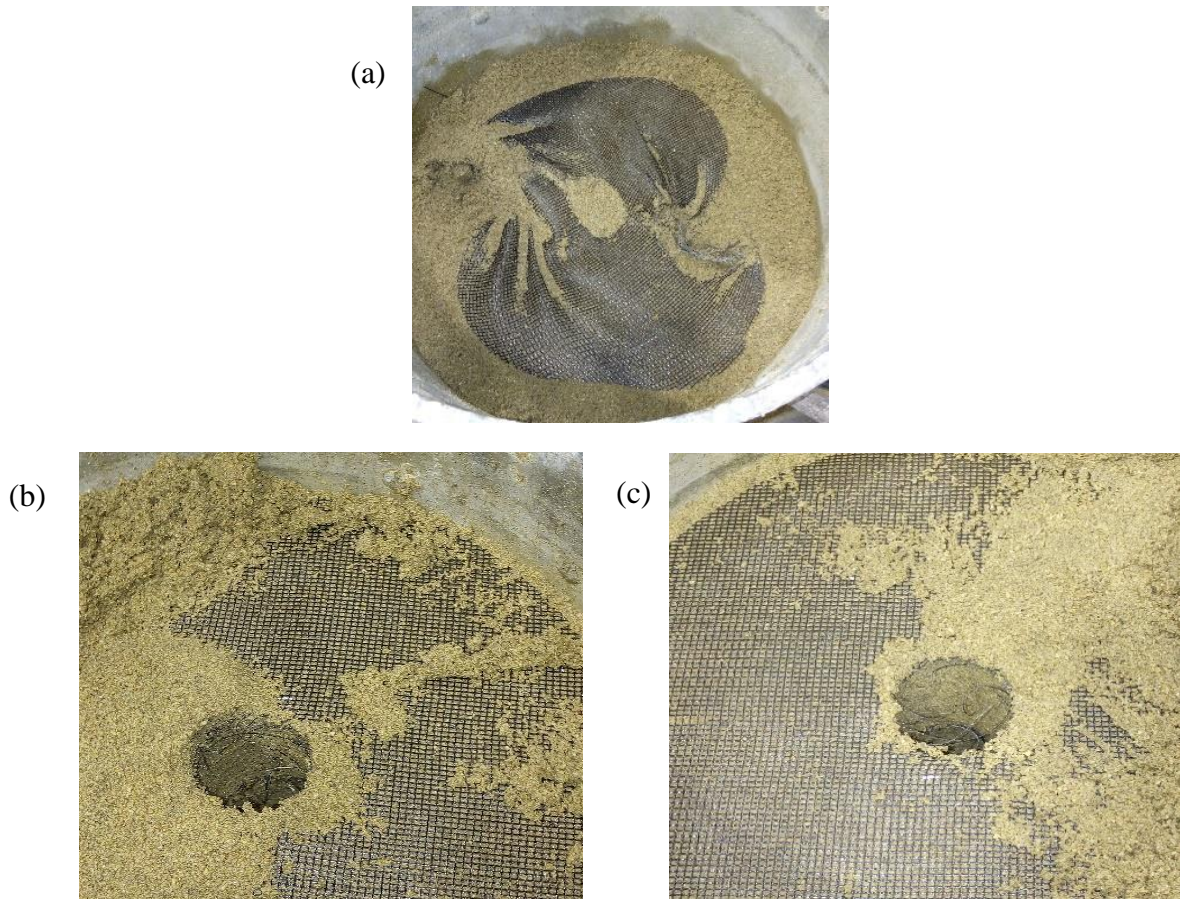


Figure 4.12: Drilled-through geo-meshes in geosynthetic-reinforced sand

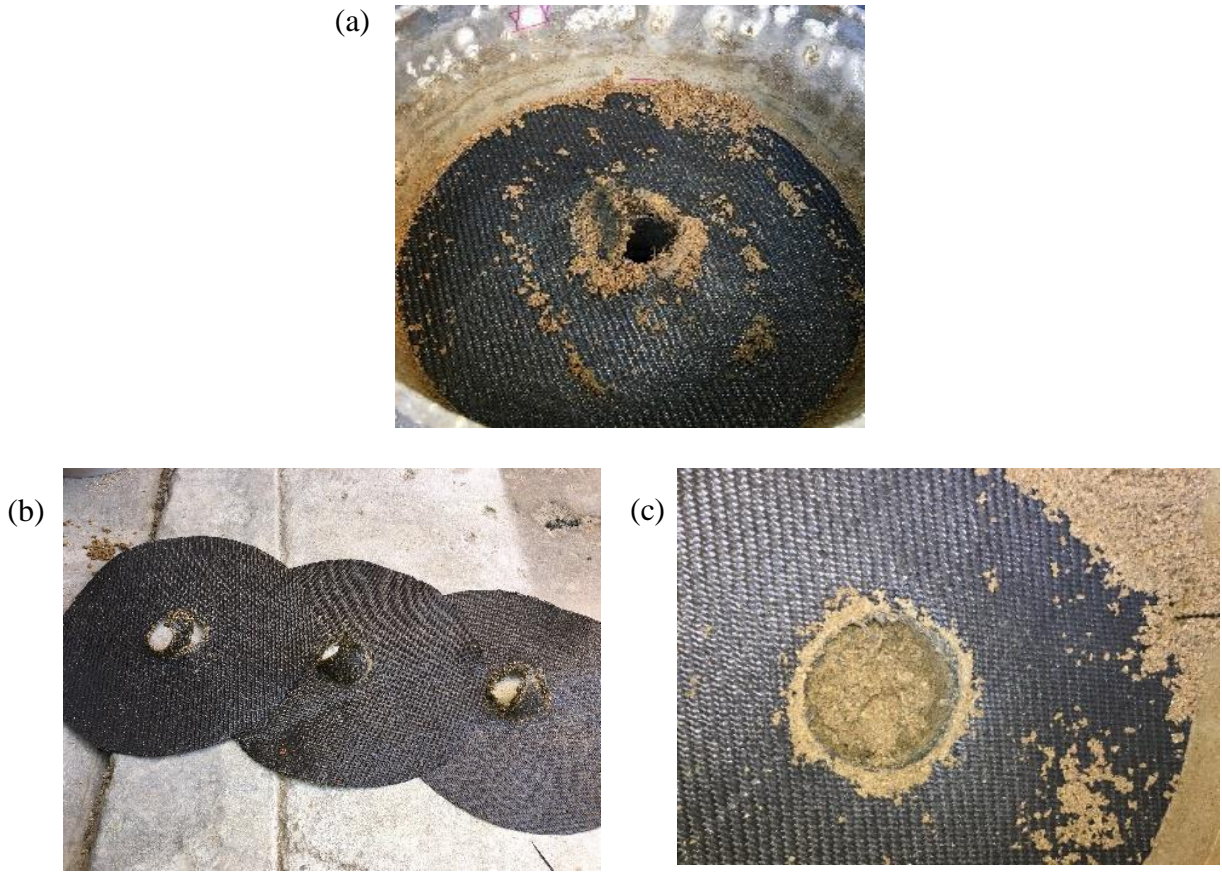


Figure 4.13: Drilled-through woven geofabrics (AMOCO 2044) in geosynthetic-reinforced sand

4.5 Setup of Initial Geostatic and Dynamic Load conditions

Owing to the strong dependence of the mechanical characteristics of soil on its effective stress state, the in-situ geostatic stress state in the computer soil model needs to be first established in an equilibrium condition under self-weight before applying other external loadings. In this study, the general load sequence on the guardrail-A-frame-GRS wall consisted generally of 3 stages as in [6]. In the first stage, gravity loading was turned on slowly in a ramp manner to set up a realistic initial stress state that is in three-dimensional static equilibrium upon which the stress-strain behavior of the soil depends. In the second stage, a distributed surface loading representing 2 feet of soil on top of the backfill was imposed where appropriate. To correspond more truly to actual TL-4 level vehicular collision impacts than what was done in the preceding development [6], the third stage of loading was changed from a prescribed impact force time history with a specific peak resultant load of 240 kN (54 kips) as shown in Figure 4.8 to one that was based on a three-dimensional finite

element simulation of the vehicular collision with the guardrail system as will be discussed in the next section.

5 SIMULATION RESULTS AND ANALYSIS

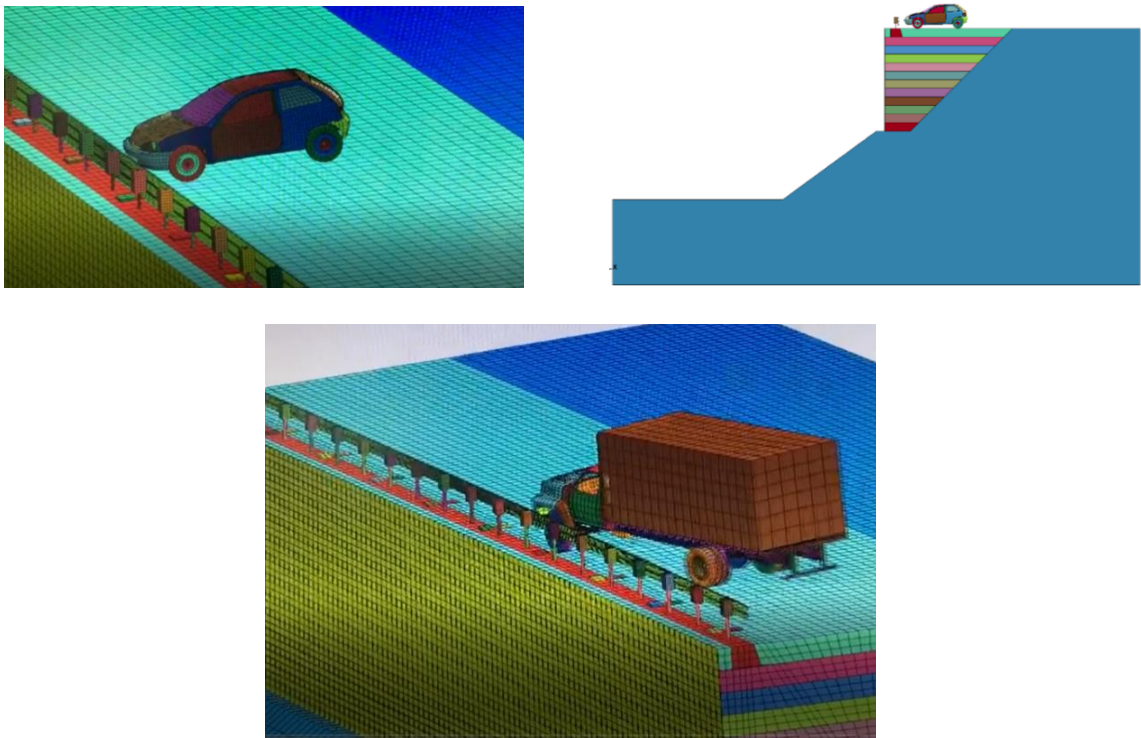


Figure 5.1: Computer models of vehicular collisions with guardrails on micropile-truncated GRS wall

Because of the number of structural and material regions of the micropile-geosynthetic reinforced soil wall and the incoming vehicle as well as the multi-point non-synchronous dynamic contact in a collision scenario, the computer model runs were time-consuming despite various analytical reductions. The results were also generally sensitive to the geometric, material, interfacial, contact and initial conditions. In the simulations conducted, large deformation, highly nonlinear elastoplastic material behavior, variable contact points/conditions as well as significant structural disintegration of vehicles in severe TL-4 type impacts were often the case. To provide the necessary degree of confidence and insight into the assembled computational model's performance in handling the complex vehicle-guardrail-foundation interaction as well as to identify a representative MASH compliant configuration of the guardrail that could provide a realistic impact load transfer to the underlying hybrid GRS wall, a number of guardrails and post configurations, material

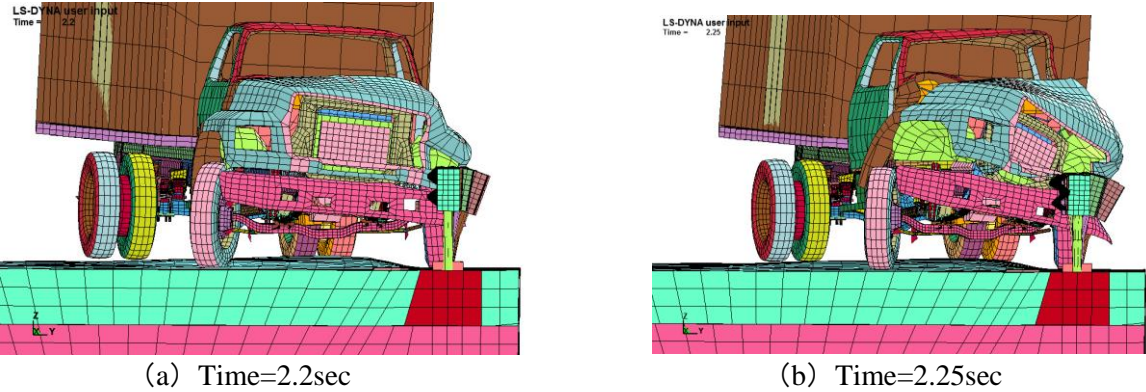
representations, collision angles and velocities were considered so as to identify the critical case for more in-depth evaluations. In what follows, key results for the purpose of validating the computational sufficiency in modeling the collision onto the roadside barrier under MASH TL-4 will be presented first, before proceeding to pertinent analysis for the assessment of the hybrid micropile-GRS wall-guardrail system.

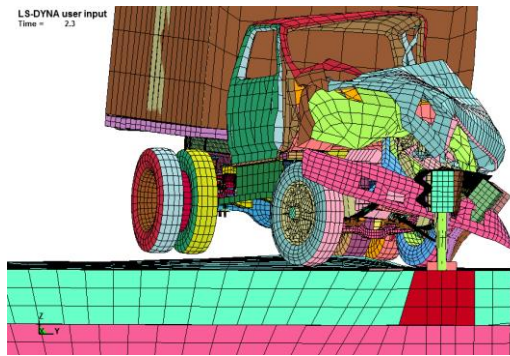
5.1 Performance Checks of Vehicle-Guardrail-Micropile-GRS Wall Model in Collision Simulations

As a basic check of the ability of the multi-domain finite element model described earlier to delineate the structural/foundation performance of the guardrail-foundation models under vehicular collisions according to MASH, preliminary simulations were conducted to confirm the performance of the simulation approach with the level of model details adopted as well as to secure some needed insights to identify the critical case to be considered in more detail. The following 3 examples are illustrative of the purpose and relevance of this phase of effort:

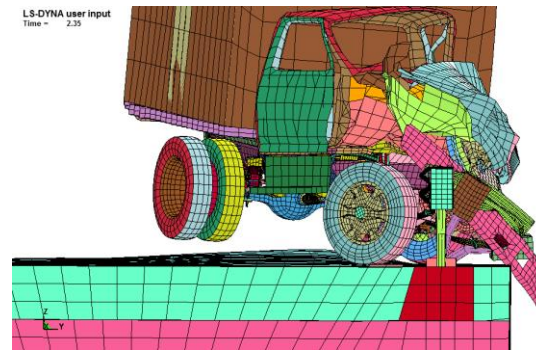
Example 1: 10000 kg single-unit truck on 36” tall W-beam guardrail @ 90km/h and 15° angle:

As a minimum height of 36” (0.91m) was recommended for MASH TL-4 compliant guardrails in some recent DOT studies, e.g., [14], a computer model with a 0.91m high W-beam guardrail defined in Section 4.3 was used in this example for MASH’s single-unit truck TL-4 condition. A set of snapshots of the resulting vehicle collision simulation is shown in Figure 5.2.

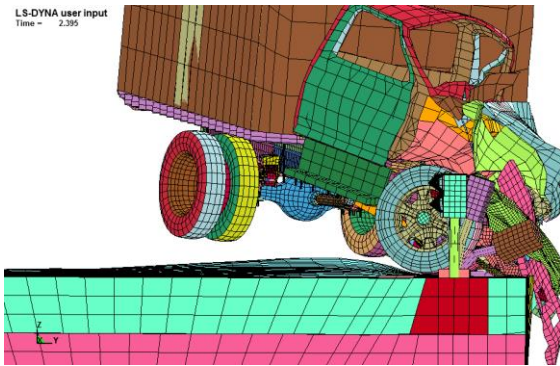




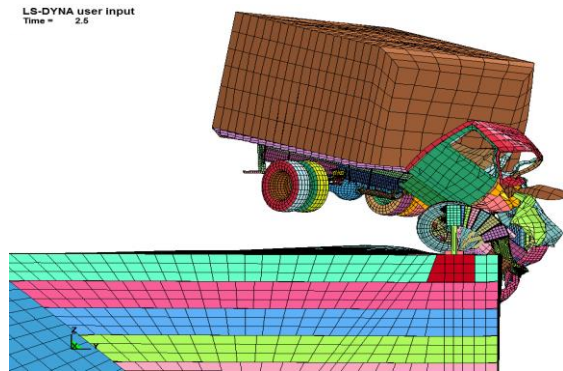
(c) Time=2.3sec



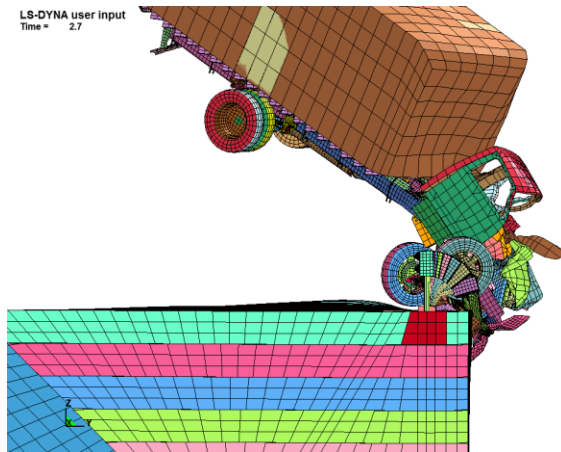
(d) Time=2.35sec



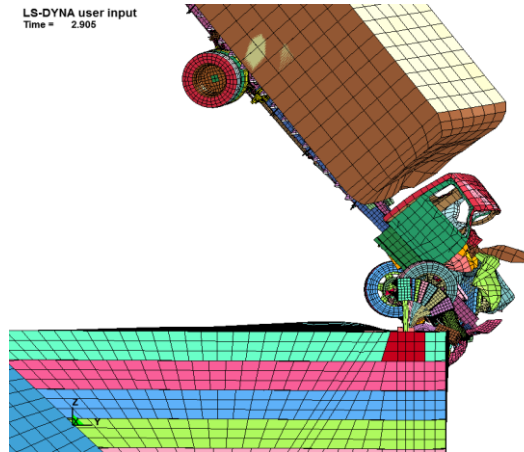
(e) Time=2.4sec



(f) Time=2.5sec



(g) Time=2.7



(h) Time=2.905sec

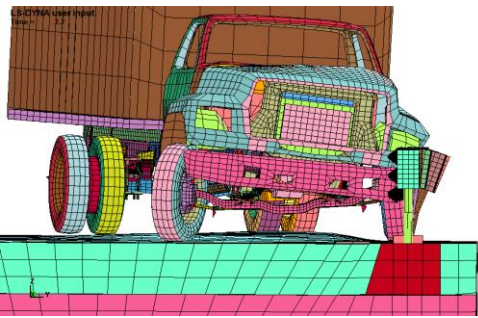
Figure 5.2: Sequential snapshots of F-800 truck colliding @ 90 km/hr and 15° oblique impact with 0.91m (36”) W-beam guardrail on a truncated GRS wall

As one can see from the display, there is a serious liftoff of the truck's body, very serious disintegration of its front engine compartment and hood, and significant damage and warping of the W-beam guardrail due to the impact. With the clear tendency of the truck to flip up and fly over

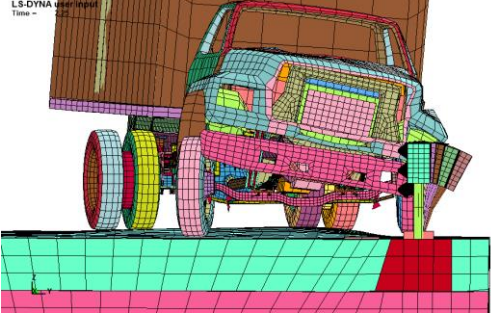
the rail as indicated by the result, it is apparent that the 0.91m (36”) high W-beam guardrail will be unable to contain the SUT, thus failing the most basic MASH’s test level 4 requirement on the guardrail.

Example 2: 10000kg single-unit truck on 36” tall thriebeam guardrail @ 90km/h and 15° angle

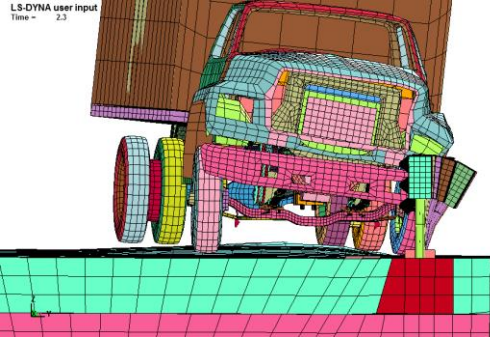
In view of the insufficiency of the guardrail configuration in Example 1, the guardrail in this example was strengthened by replacing the W-beam by the thriebeam described in Section 4.1. Subjecting it to the same impact load from the 10000kg Ford F-800 under the required MASH TL-4 condition, a snapshot sequence of the collision simulation is shown in Figure 5.3. Comparing the response shown in Figure 5.3 to Figure 5.2, it was found that the truck’s tendency to flip up was considerably less because of the stronger thriebeam guardrail, representing a noticeable improvement over the W-beam guardrail. Nonetheless, its performance would still be considered as marginal at best under MASH.



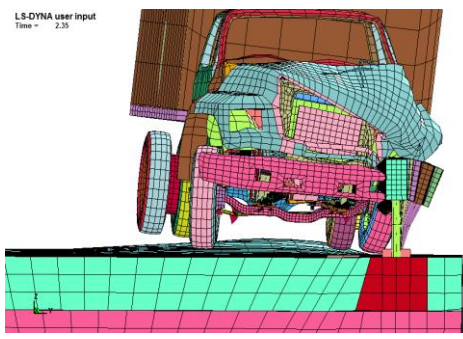
(a) Time=2.2sec (v=90 km/h)



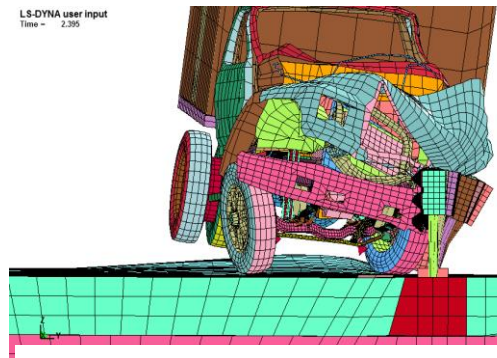
(b) Time=2.25sec (v=90 km/h)



(c) Time=2.3sec (v=90 km/h)



(d) Time=2.35sec (v=90 km/h)

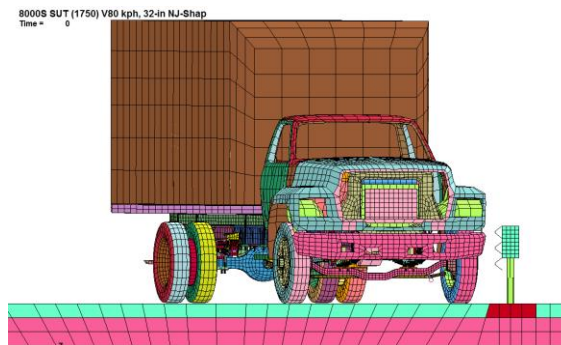


(e) Time=2.4sec (v=90 km/h)

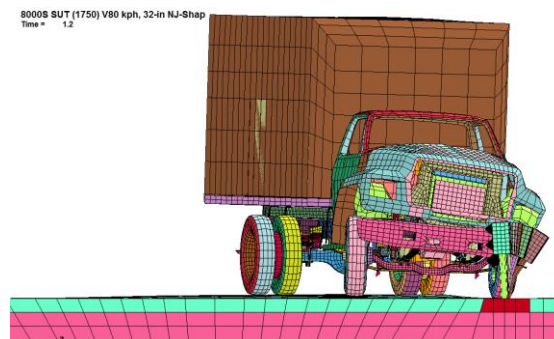
Figure 5.3: Sequential snapshots of F-800 truck colliding @90 km/h & 15° with 0.91m (36”) thriebeam guardrail on micropile-truncated GRS wall

Example 3: 10000kg single-unit truck on 36” tall thriebeam guardrail @ 80km/h and 15° angle

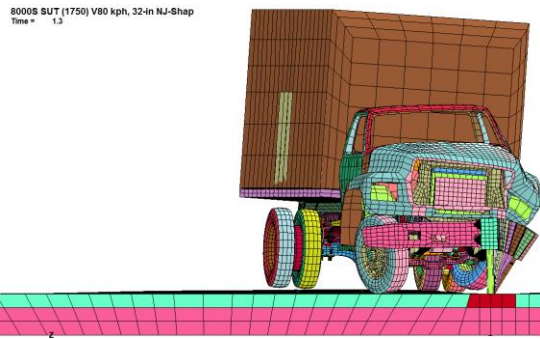
To gain further insights beyond those from Examples 1 and 2, the speed of the truck in this case was reduced from MASH’s 90 kmh (56 mph) to 80 kmh (50 mph) in this example. The 50 mph speed was chosen for several reasons: (i) it is identical to the speed specified in NCHRP-report 350’s standards for trucks, (ii) it helps to elucidate the degree of sensitivity of the collision simulation with respect to a vehicle’s speed, and (iii) it provides a basis and insights on the demand of MASH relative to past AASHTO requirements on roadside hardware. The collision snapshot sequence of the time progress of the collision progress of this example is shown in Figure 5.4 below.



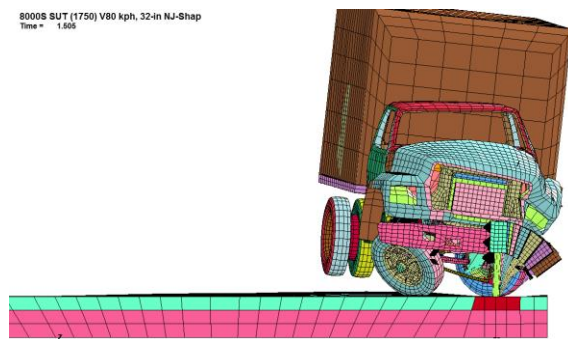
(a) Time=0 h=0.91m



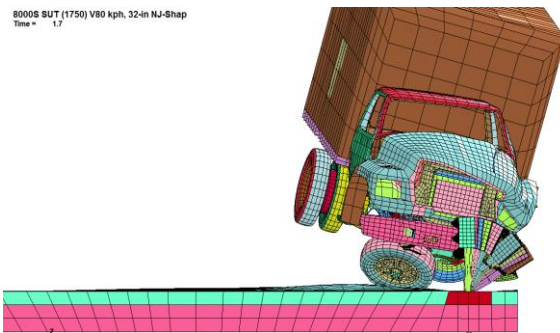
(b) Time=1.2s h=0.91m



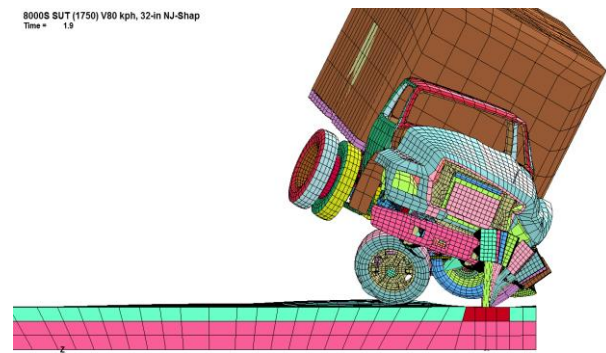
(c) Time=1.3s (v=80 km/h)



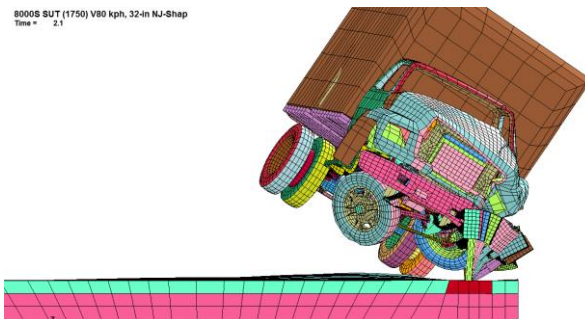
(d) Time=1.5s (v=80 km/h)



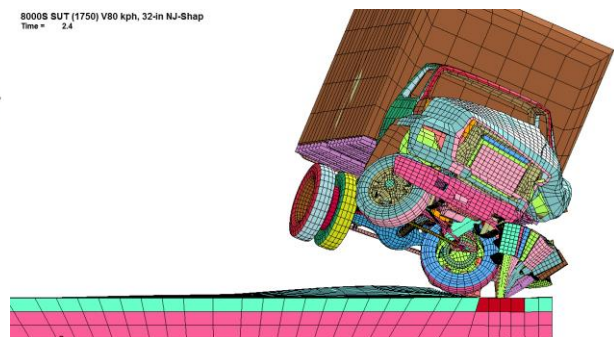
(e) Time=1.7s (v=80 km/h)



(f) Time=1.9s (v=80 km/h)



(g) Time=1.7s (v=80 km/h)



(h) Time=2.4s (v=80 km/h)

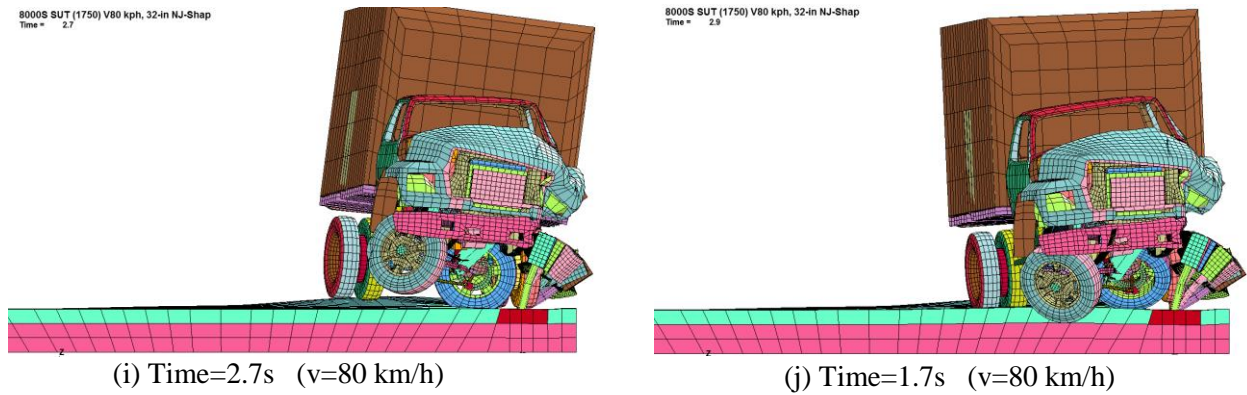


Figure 5.4: Sequential snapshots of F-800 truck colliding @80 km/h & 15° with 0.91m (36'') thriebeam guardrail on micropile-truncated GRS wall

As illustrated in Figure 5.4 for this case, while the 10000kg truck at 50 mph speed still had the tendency to flip up momentarily, it was able to come back down and be re-directed back to the road after impact. Taking into account that the weight of truck (10000 kg) in this example is about 20% heavier than what was prescribed in NCHRP-350 standard, the thriebeam guardrail should qualify as acceptable by the NCHRP-350's standards, as evidenced by its past adoption by a number of DOT agencies. With the current MASH's TL-4 standard that requires guardrail performance under a truck speed of 90 kmh as employed in Example 2, however, it was evident that it would be prudent to employ an improved guardrail to ensure an adequate simulation of the level of collision impact load-transfer to the underlying hybrid micropile-GRS wall system.

Being generally consistent with related past studies and crash tests (e.g., [13, 14]), the observations from the foregoing examples lent credence to the adequacy of the level of three-dimensional nonlinear finite element modeling for the proposed assessment of the hybrid GRS wall under MASH. For the project's focus, two key insights from the preceding examples are particularly relevant. The first is that the simulation platform assembled and employed is generally sufficient to distinguish and delineate the performance of the guardrail under severe vehicular impact such as those resulting from Test Level 4 crashes by MASH. The second one is that the 36'' height of the guardrail, even if it were made of thriebeams, is still likely not sufficient to meet the current standards in MASH of being able to retain and re-direct the truck back to the road, and therefore not suitable for the evaluation of the hybrid micropile-GRS foundation wall's adequacy as the support for a MASH compliant roadside barrier. In recognition that the impact performance of the

underlying micropile-GRS wall should be checked against a guardrail design that at least satisfies the strength and stability criteria of MASH, a taller thriebeam guardrail was subsequently considered as a more realistic and prudent option. To this end, the height of the thriebeam guardrail for the truck case was raised from 36" (0.91m) to 40" (1.01m) for the single-unit truck case. The choice was arrived at because it is a height that is apt to be sufficient to retain and re-direct the truck back to the road, yet the resulting bottom edge of the thriebeam is low enough to be effective in stopping a passenger car from under-riding it. As will be discussed in the following section, the taller guardrail choice was indeed found to be able to meet the expectation and thus formed a credible basis to assess viability of the hybrid micropile-truncated GRS wall under MASH's elevated collision conditions.

5.2 Vehicular Collision Loads on 40" Steel Guardrails on Hybrid Micropile-GRS wall

Focusing on the 40" (1.01m) high thriebeam guardrail design henceforth as a reasonable baseline roadside guardrail representation for the evaluation of the hybrid wall design's adequacy under severe collision impacts stipulated by MASH, the analytical capability of the finite element simulation platform that was illustrated by the preceding examples was used to analyze several relevant vehicle-guardrail-roadside hardware and foundation scenarios. Comparing the impact load on the guardrail and foundation from a passenger car versus that from a truck collision for example, the expectation that the truck impact would be the most critical case was confirmed. As illustrations, selected results of both the car and the truck cases pertinent to the adequacy assessment of the hybrid wall design are presented in the following 3 sub-sections.

5.2.1 Oblique Passenger Car Impact

For the case of the Geo Metro having a 25° oblique impact at 62 mph (100km/h) with a steel thriebeam barrier (i.e. at MASH's TL-4 condition) that was anchored to the grade beam of the hybrid GRS wall (see Figure 5.5), it was found that the guardrails of 36" (0.91m) and 40" (1.01m) heights could both successfully re-direct the car back to the road although the front of the car suffered significant crushing and damage. For the assessment of the hybrid wall, the level of lateral displacements and impact force are the key items of engineering interest. In Figure 5.6 where the horizontal/lateral displacement δ_h 's time history of the guardrail upon impact is shown, it is shown that it has a peak of 0.37m and a residual value of 0.12m relative to the geostatic state. As shown

in Figure 5.7 where the resultant lateral impact force F_h 's time history is plotted, the thrust reaches a peak of about 230 kN (52 kips) and subsides at a time of 0.58s sec after the initial contact, with a major outward resultant occurring over a duration of 0.16 sec. One can also see from the figure that the guardrail had a couple of moments of inward pull (i.e., F_h turned tensile) after the large outward impulse. Through an examination of the time sequence of the simulated collision event, the result was found to be the consequence of the car getting partially entangled with the corrugated thriebeam guardrail, a phenomenon similar to the snagging interaction problem between some structural parts of the vehicle and the rail system in reality. As one may expect, the simulation also showed that the vehicle in oblique impact will not only cause the guardrail to deflect flexurally upon the thrust of the car but the vehicle itself will slide or bump along it upon collision before stopping, i.e., shifting the load reactions from one span/post to the next. Of engineering interest as well is that the peak impact thrust of 230 kN (52 kips) is comparable to NCHRP-350's recommended value of 240 kN (54 kips). As the Geo Metro is lighter than the passenger car's specification of MASH, however, this case should be taken as a validation of the computer simulation platform similar to those discussed in Section 5.1 rather than an adequacy test of the wall design for MASH.

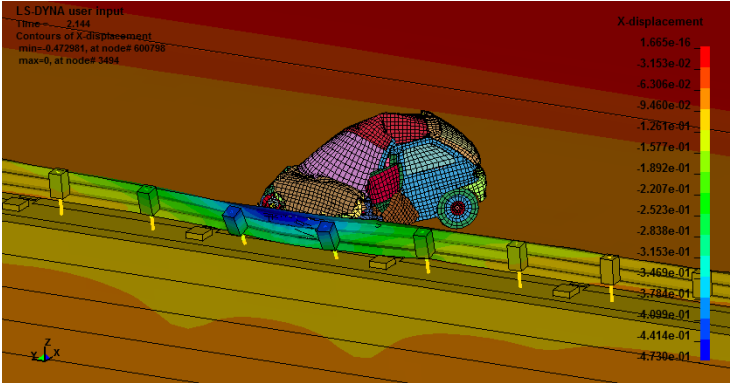


Figure 5.5: Passenger car colliding with thriebeam guardrail on micropile-GRS wall

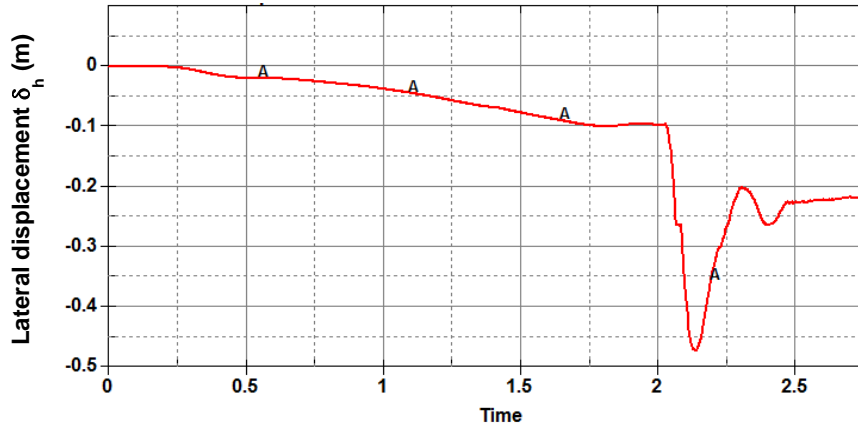


Figure 5.6: Top lateral displacement time history of 36'' (0.91m)-high thriebeam beam guardrail under 25° oblique 100km/hr car impact: Peak $\delta_h = 0.31\text{m}$

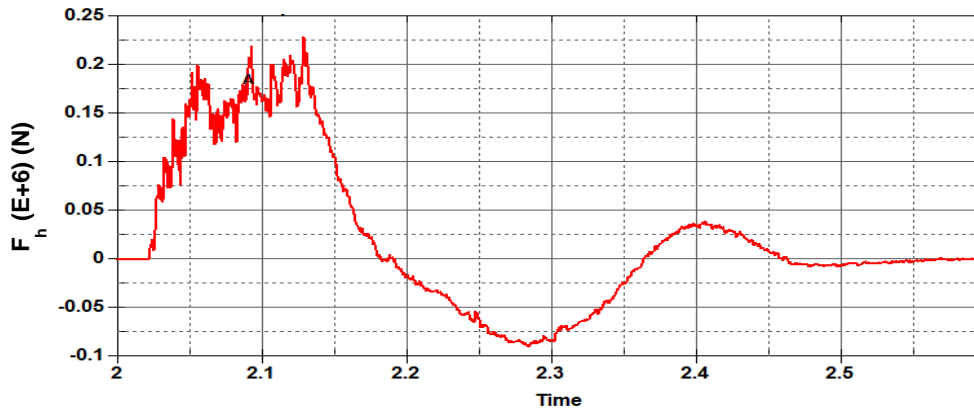


Figure 5.7: Resultant impact force F_h time history from 25° oblique 100km/h car impact on 36'' (0.91m) high thriebeam guardrail: Peak thrust=230 kN (52 kips)

5.2.2 Oblique Single-Unit Truck Impact

As illustrated in the examples in Section 5.1, the severity of the truck collision impact could not be handled well by the 36'' (0.91m)-high thriebeam guardrail under MASH's TL-4 condition. With the thriebeam height in the model raised to 40'' (1.01m), however, the LS-DYNA simulation showed that a 90 kmh (56 mph) Ford F-800 truck in 15° oblique collision with the guardrail could be contained and re-directed back to road as required by MASH, even if there were some minor snagging problems. With the strong potential that the taller guardrail design would be MASH compliant, an examination of key quantitative measures of the response of the guardrail and the geosynthetically reinforced soil backfill and foundation is in order. To this end, the displacement response of the guardrail at both the top and anchorage levels, as well as the resultant impact force

time histories transmitted by the vehicle as a result of the collision impact are shown in Figure 5.9 and Figure 5.10.

From the first figure's time history of the top lateral displacement δ_h of the guardrail, one can see that the impact-induced peak value for the top of the guardrail post is 0.51m with a residual value of 0.32m relative to the geostatic value as a result of the elastoplastic behavior of the steel sections. The resultant impact force time history shown in Figure 5.10 shows that its peak value is about 390 kN (88 kips) (occurring at 0.23s after first moment of contact), with the duration of the major lateral impulse being about 0.35 sec. Substantiating that the truck TL-4 impact case is much more severe than the passenger car case, one may note that (i) the value of 390 kN as the peak thrust level is significant higher than the 230 kN peak in the passenger car case/Geo Metro case in oblique 25° impact, and (ii) the duration of 0.35 sec of the major outward impact's duration in the SUT case is also longer than the 0.16 sec of the passenger car case in Section 5.2.1. These observations helped to confirm that a SUT's collision with a 40"-high thriebeam guardrail can be considered as the critical case for the evaluation of the hybrid foundation wall system under MASH TL-4 condition. For its direct relevance to the hybrid wall's reaction, the displacement time history at the base of the rail post is also plotted in Figure 5.9. It shows that at the anchorage level of the support rail post to the grade beam, the peak displacement from the truck impact is 0.025m with a residual value of 0.015m. Both of these magnitudes are small and within normal acceptable limits to the hybrid wall structure, illustrating the benefit of the added stiffness and resistance from the micropile A-frame system.

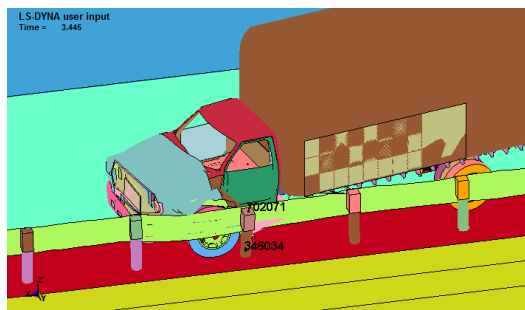


Figure 5.8: Single unit truck running into 40" (1.01m)-high thriebeam guardrail on micropile-MSE wall at 90 kmh and 15° angle

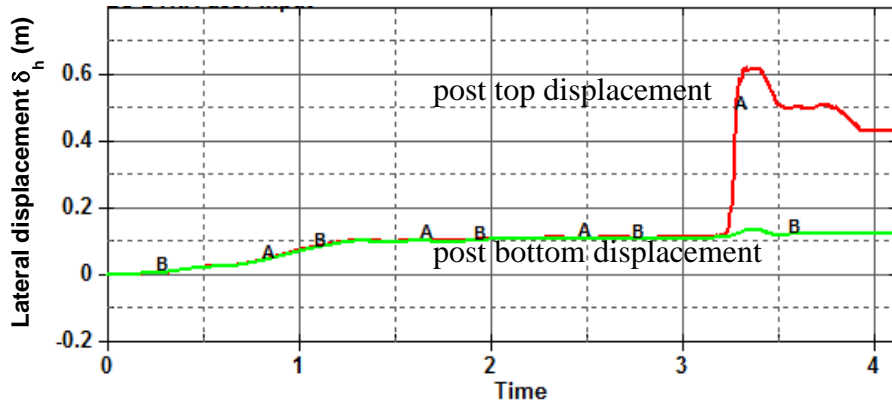


Figure 5.9: Top and bottom guardrail post displacements from 90 kmh -15° oblique truck collision on 40” thriebeam-pile-GRS wall

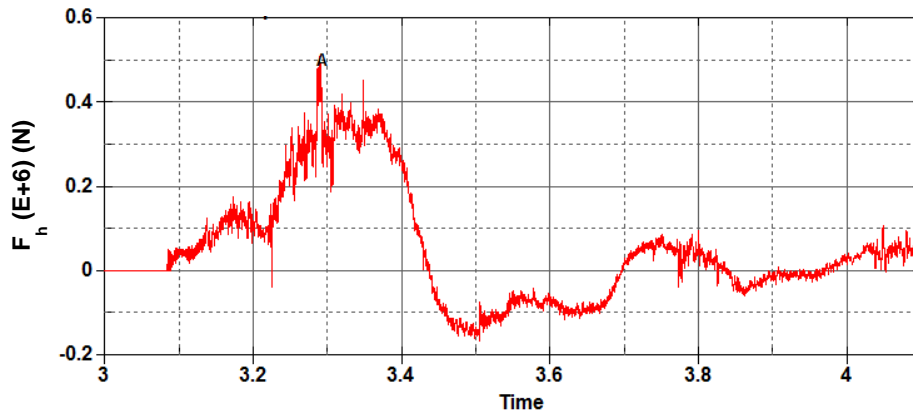


Figure 5.10: Resultant impact force F_h time history from 90 kmh -15° oblique truck collision on 40” thriebeam-pile-GRS wall: Peak thrust =390kN (88 kips)

5.2.3 Equivalent-Frontal Single-Unit Truck Impact

To provide further insight and a quantitative basis to relate MASH to past NCHRP-350's standards and resistance requirements, the possibility of an equivalent direct frontal (90°) collision impact was deemed as an item of comparable engineering interest for this study. To this end, computer simulations were also conducted for a F-800 truck in 90° frontal impact with a velocity equal to the normal component of the oblique impact case, i.e., $90\text{kmh} * \sin 15^\circ$ onto the thriebeam guardrail (see Figure 5.11).

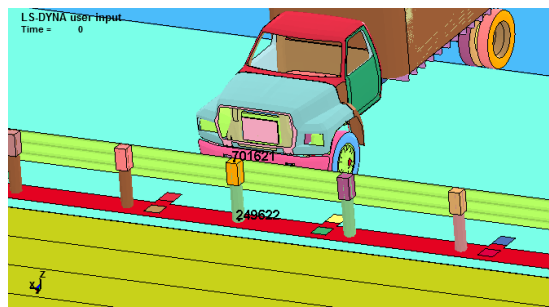


Figure 5.11: Single unit truck running into 40”(1.01m) high thriebeam guardrail on micropile-GRS wall under 90° equivalent-frontal impact

The key results for the post's top and bottom displacements as well as the impact force resultant are shown in Figure 5.12 and Figure 5.13, respectively. As can be seen from Figure 5.12, the peak top displacement of the guardrail post is 0.43m, with a residual value of 0.33m relative to the geostatic value. They are quite comparable to the 15°-oblique SUT impact case's 0.51m and 0.32m, respectively as discussed in Section 5.2.2. From the impact force resultant time history shown, one can see that the time variation from the equivalent frontal impact is considerably simpler than the one for the oblique MASH case, with its peak thrust level of 425 kN (96 kips) being somewhat higher than the 390 kN (88 kips) peak value in the MASH oblique impact case. At the base level of the post which is anchored into the grade beam, the peak and residual displacement are 0.024m and 0.012m, respectively. They are also comparable to the corresponding values of 0.025m and 0.015m from the computed response shown in Figure 5.9 and Figure 5.10 for the true 15° oblique MASH case.

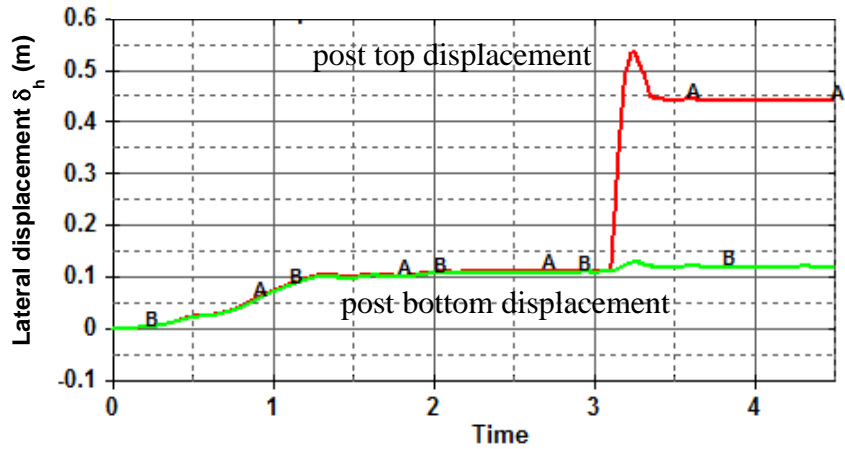


Figure 5.12: Top and bottom 40” guardrail post displacements from $90\text{kmh} \cdot \sin(15^\circ)$ equivalent-frontal truck collision on 40” thriebeam-pile-GRS wall

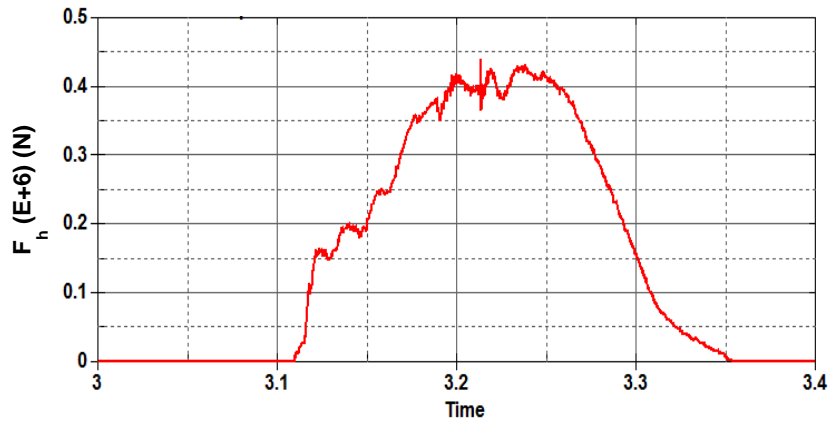


Figure 5.13: Resultant impact force F_h time history from $90\text{kmh} \cdot \sin(15^\circ)$ equivalent-frontal truck collision on 40” thriebeam-pile-GRS wall: Max=425kN (96 kips)

5.2.4 Soil Deformation in Hybrid GRS backfill from TL-4 Truck Impact

For the assessment of the adequacy of the hybrid GRS design, the level of deformation in the GRS soil backfill region as a result of the vehicular collision is of equal relevance. To this end, a three-dimensional display of the spatial distribution of the von Mises or *effective strain* which is a scalar overall measure of the magnitude of the deviatoric or shear component of the 3D strain tensor of the soil medium is useful. Defined by

$$\varepsilon_{effective} = \frac{\sqrt{2}}{3} \sqrt{(\varepsilon_1 - \varepsilon_2)^2 + (\varepsilon_2 - \varepsilon_3)^2 + (\varepsilon_3 - \varepsilon_1)^2}$$

where ε_i are the principal strains, its variation at the initial geostatic, peak response and the residual states obtained from the simulations are shown in Figure 5.14 to Figure 5.16, respectively. Comparing Figure 5.15 to Figure 5.14, one can see that the change in the peak $\varepsilon_{effective}$ due to the collision is about 0.87%. Likewise, a comparison of Figure 5.16 to Figure 5.14 indicates that the residual $\varepsilon_{effective}$ is about 0.18%. Both of these strain levels are small and acceptable with reference to common foundation engineering design practice.

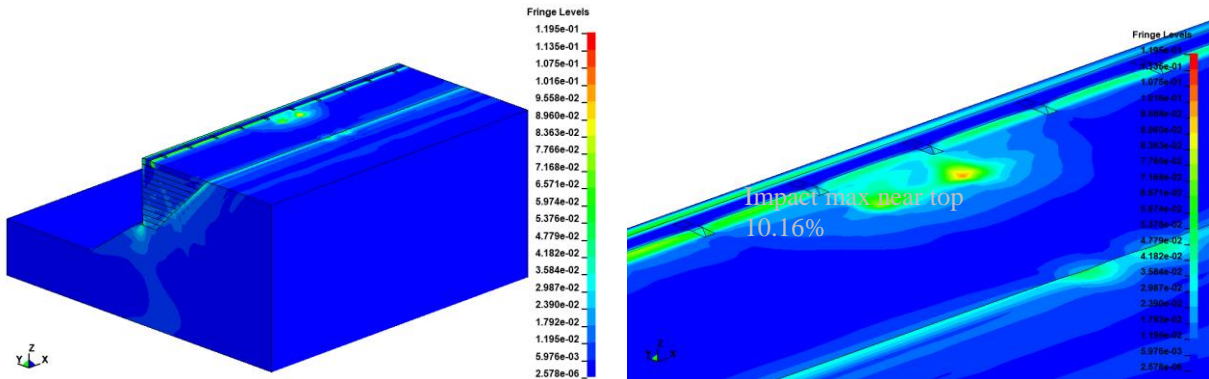


Figure 5.14: Effective strain variation under in-situ geostatic condition:

$$\varepsilon_{in-situ\ max} = 11.95\%$$

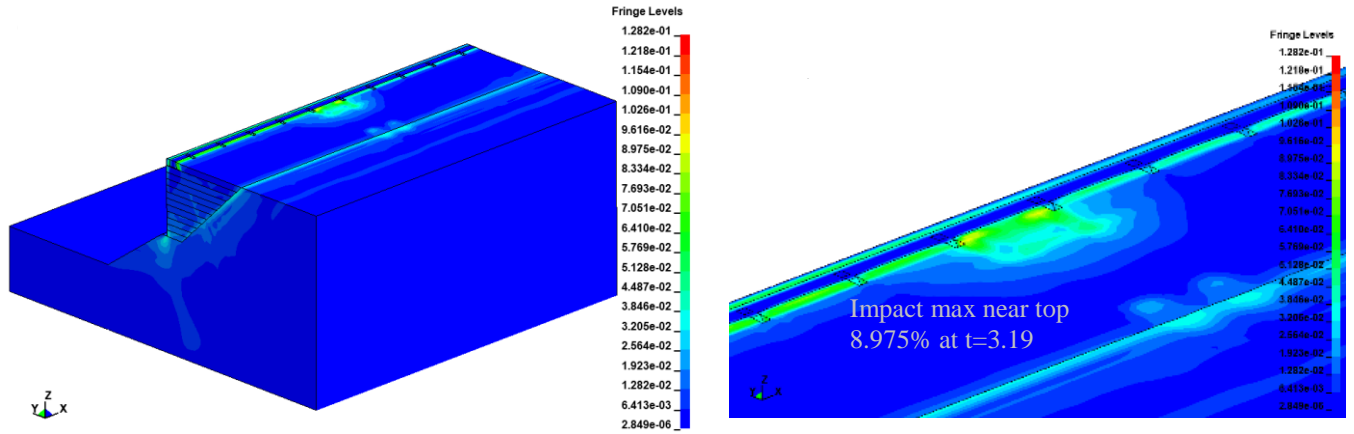


Figure 5.15: Effective strain variation from effective frontal truck impact load

$$\epsilon_{\text{effective impact max}} = 12.82\%$$

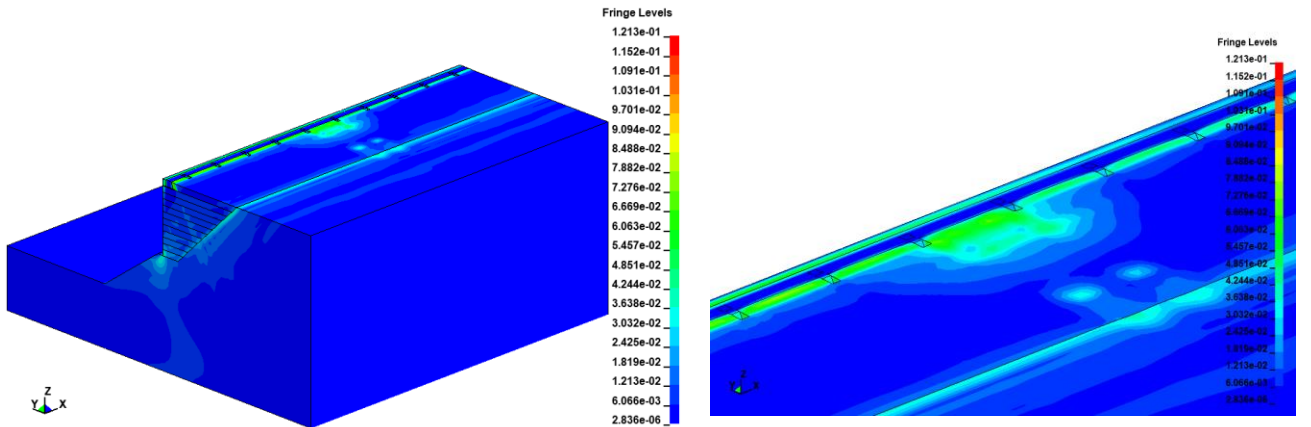


Figure 5.16: Residual effective strain variation from effective frontal truck impact load:

$$\epsilon_{\text{effective residual max}} = 12.13\%$$

Also noteworthy is that they are only slightly higher than the peak and residual strains of 0.6% and 0.15% in the same hybrid wall design found in Fig. 5.22 of [6] for the NCHRP-350 impact condition of 240 kN impact thrust. The fact that the peak strain increment of 0.87% under MASH is above the one subjected to NCHRP-350 is certainly reasonable. The small increases in the deformation of the GRS backfill from both MASH and NCHRP-350 impact conditions illustrate again the result of the extra stiffness and load resistance provided by the installation of the concrete gradebeam-micropile A-frame system.

5.3 Displacement of Hybrid Wall and Foundation from Impact

With the increased weight and speed of vehicles under MASH as illustrated in the preceding sections, other measures of the performance of hybrid wall in other aspects under much higher lateral dynamic thrust are also of interest. With the resultant impact force results shown in the preceding sections, either 390 kN from oblique impact or 425 kN from effective frontal impact can be considered as a design target for the hybrid micropile-GRS wall assessment. To evaluate the hybrid wall's adequacy for such conditions, the design charts developed in [6] for the hybrid micropile-GRS wall under 5 different levels of direct frontal impact load from 120 to 600 kN (see Figure 5.17) are useful. With the effective frontal collision yielding a conservative estimate of a peak force level as 425 kN (96 kips) relative to the oblique impact case's 390 kN (88 kips), the chart in Figure 5.18 for determining the barrier lateral displacement as a function of the peak impulsive load level from [6] is applicable. In the figure, the "pile" in the legend stands for the "hybrid A-frame micropile-GRS wall" case while "no pile" stands for a "regular GRS wall." From Figure 5.18, one can see that the peak and residual displacements using 425 kN as the lateral design impact load are about 0.03m and 0.02m, respectively. These are comparable to the corresponding results of 0.025m and 0.015m from the finite element MASH TL-4 oblique impact simulation for a single-unit truck as they are noted in Section 5.2.2. The small post-base displacements show that the stronger structural-foundation configuration allows the impact loads on the barrier in both cases to be mostly taken up by the micropiles and grade beam which in turn transfer them to the GRS in a more distributed manner. Their similarity in the response level also suggests that the representation of the impact load as a unilateral impulse with a peak force in frontal impact can, with suitable calibration, lead to comparable final design but with less computational complexities relative to a full-fledged oblique collision simulation.

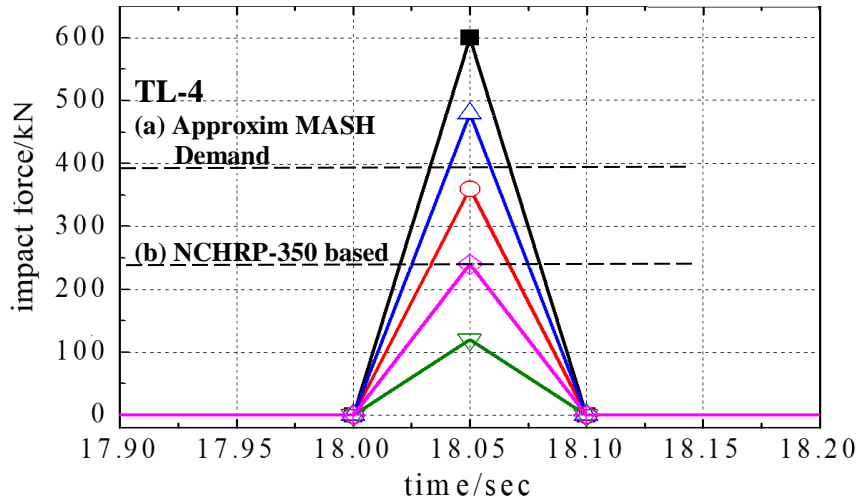


Figure 5.17: Simplified impact load time histories for hybrid micropile-GRS wall assessment and design

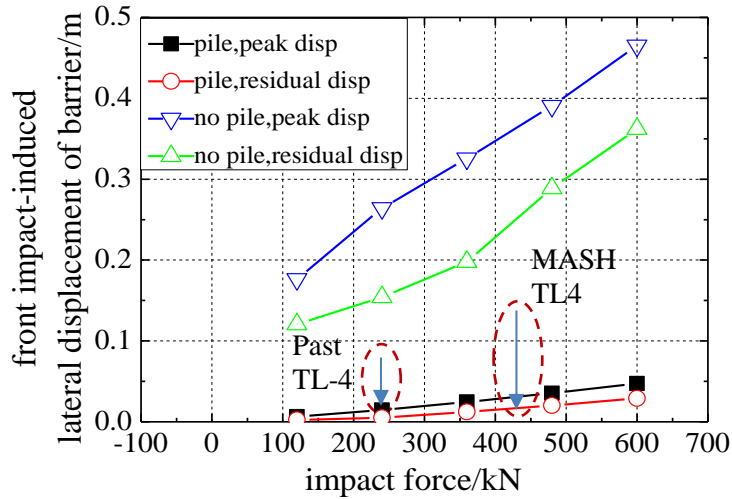


Figure 5.18: Barrier lateral displacement under different frontal impact load levels [6]

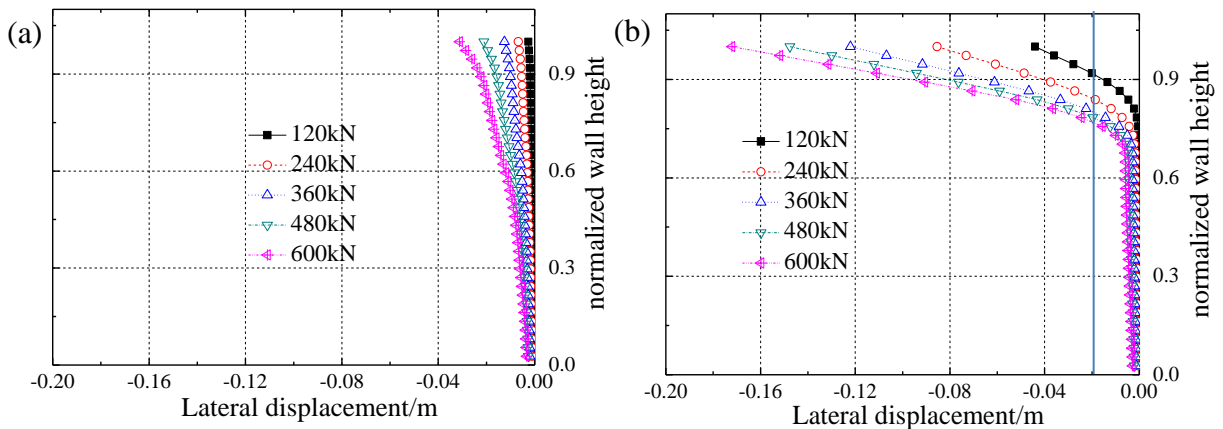


Figure 5.19: Lateral displacement of front wall panel by different impact force levels: (a) hybrid GRS wall, (b) regular GRS wall [6]

To assess the performance of the hybrid micropile-GRS design under MASH TL-4 for SUTs, another measure is the lateral movement of the wall's front concrete panel. The results for a hybrid micropile-GRS wall in terms of peak and residual deflections of the concrete facing under the range of impact level are shown in Figure 5.19a. As a result of the reinforcement by the micropile A-frames, the lateral deflection of the wall panel of hybrid micropile-A-frame-GRS wall is also minimal along the whole height of the wall. By interpolation, the hybrid wall's displacement is 0.018m (1.8 cm) for a peak impact force level of 425 kN which corresponds to MASH TL-4 condition for SUTs. This is in contrast to the displacement level of 13.7cm in the case of an ordinary GRS wall without micropiles as shown in Figure 5.19b. This amounts to an approximately 87% reduction by virtue of the hybrid micropile-GRS wall design, illustrating the stiffening effect provided by the micropile A-frame in the truncated GRS wall in face of MASH.

6 IMPLEMENTATION OF RESEARCH TO ENGINEERING PRACTICE

The results from this study can be used as the basis by CDOT to update the worksheets, such as possibly waiving the requirement of the sacrificial PVC pipe installation in the GRS of the hybrid wall system to reduce the construction details and time. Examples of relevant candidates are Worksheet B-504-A3, A5 and V2 shown in Figure 6.1 to Figure 6.3. To minimize the risk of concrete road slab cracking due to delayed backfill settlements of the soil relative to the micropiles, the determination of a suitable waiting period before completing the construction of the grade beam and pavement is advisable. Suitably selected geosynthetics for the hybrid GRS region is also recommended.

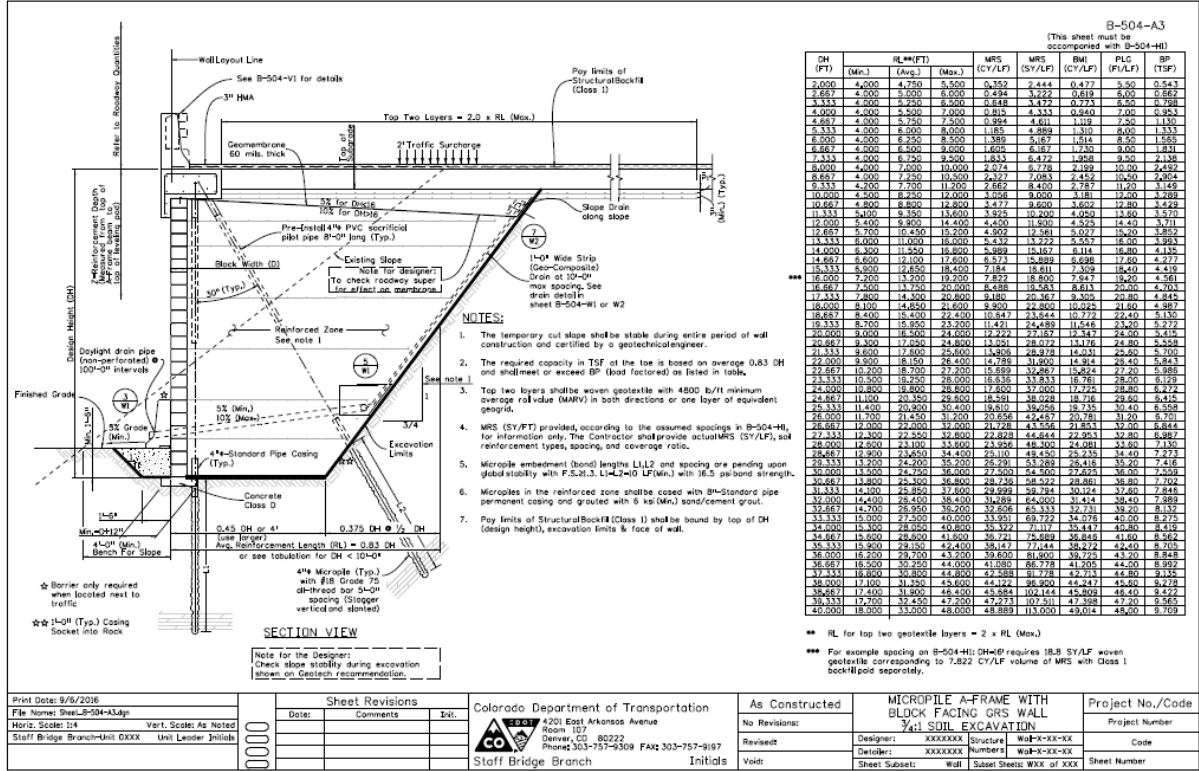


Figure 6.1: CDOT Worksheet_B-504-A3

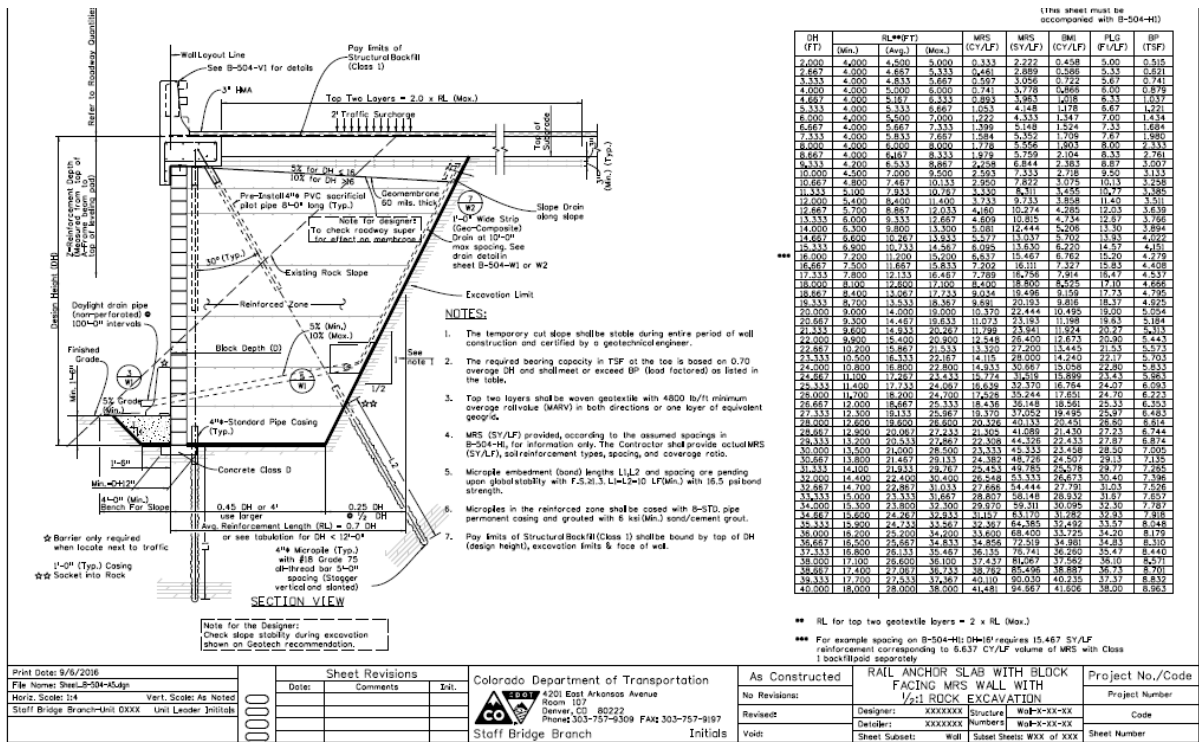


Figure 6.2: CDOT Worksheet_B-504-A5

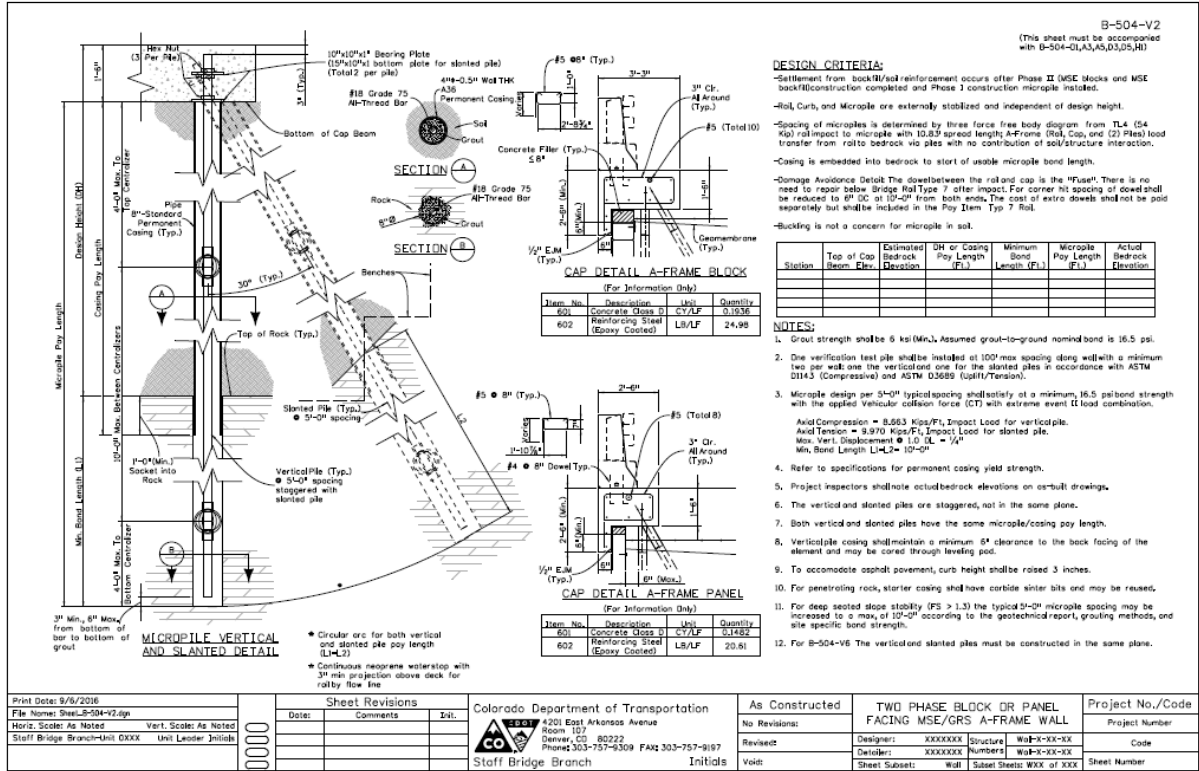


Figure 6.3: CDOT Worksheet_B-504-V2

7 CONCLUSIONS AND RECOMMENDATIONS

This report presents the result of the evaluation of the adequacy and ability of the hybrid micropile A-frame geosynthetic reinforced wall in a truncated configuration to support steel bridge guardrails under the latest AASHTO-MASH Test-Level 4 impact loading. By means of the nonlinear geometric and material modeling capability of LS-DYNA and two finite element vehicular modules developed by NCAC, a computer simulation platform was developed for modeling the guardrail interactive collision load-transfer interaction problem which involved severe structural deformation and disintegration. Parallel to the computational effort, a laboratory scaled-model study was also conducted to explore possible pile installation effects on geofabrics and soil from drilling. The possibility of an equivalent-frontal collision impact condition to facilitate the design optimization of roadside hardware was also explored. Below is a summary of the key findings from the study:

- The finite element simulation platform employed was effective in providing a realistic representation of the complex collision interaction between the vehicles, guardrail, post and the foundation.
- From the simulation and analysis, the existing hybrid micropile-truncated GRS wall design was found to be within its capacity to support MASH compliant steel guardrail design for TL-4 collision.
- To allow for more general collision scenarios including snagging, a lateral design impact load of 88 kips and a minimum height of 40” for the steel guardrail is recommended.
- Sufficient overburden stress level with a slightly moist soil condition are conducive to effective drilling through GRS.
- Woven geosynthetics for the GRS backfill should be preferable in micropile installation to mesh- or grid-type geo-reinforcements according to the laboratory study.
- An integrated steel guardrail-post-wall-anchorage design offers multiple options to meet performance targets of MASH through the variety of choices for beam sections, post dimensions, anchorage and foundation support.

Derived from the research development process and insights gained, the following actions are recommended:

- For a small increase in cost but significant improvement in safety, it is worth replacing current W-beam guardrails by thriebeams especially for curved mountain roads without shoulders.

- Other innovative hybrid designs for new construction or remedial strengthening of GRS retaining walls, embankments and curved roads using micropiles under challenging site or increasingly severe weather-induced conditions should be explored for improving Colorado's transportation infrastructure resilience.
- With the realism of 3D computer modeling capabilities demonstrated in the study, the extension of the simulation-based approach to evaluate or improve CDOT's bridge rail transition designs such as CDOT's Type G and H is highly recommended.
- To achieve the desired overall guardrail's performance, an upgrade of the post anchorage or connection details to concrete curbs, parapets, grade beam, wing wall, moment slab and beam-deck systems is warranted in view of concrete/rebar damages that appeared in some past crash tests under MASH's conditions.
- A basic field test or additional laboratory study to confirm the micropile-GRS-barrier synthesis and experimental findings from the study is highly recommended.

8 REFERENCES

- [1] Ross HE, Sicking, DL, Zimmer RA and Michie JD, Recommended Procedures for the Safety Performance Evaluation of Highway Features, National Cooperative Highway Research Program (NCHRP) Report 350, TRB, 1993.
- [2] Tom Armour, Paul Groneck, James Keelev and Sunil Sharma. Micropile Design and Construction Guidelines, Priority Technologies Program (PTP) Project, FHWA-SA-97-070, 2000.
- [3] Morrison KF, Harrison F.E, Collin JG, Dodds A and Arndt B, Shored Mechanically Stabilized Earth (SMSE) Wall Systems Design Guidelines, Publication No. FHWA-CFL/TD-06-001 February 2006.
- [4] Bligh RP, Briaud JL, Kim KM, and Abu-Odeh, A, Design of Roadside Barrier Systems Placed on MSE Retaining Wall, NCHRP Project 22-20 Report 663, 2010.
- [5] Elias, V, Christopher, BR and Berg RR, Mechanically Stabilized Earth Walls and Reinforced Soil Slopes Design and Construction Guidelines, FHWA-NHI-00-043, NHI course No. 132042 March 2001.
- [6] Pak RYS and Zhang ZC, Hybrid A-Frame Micropile-Geosynthetic Reinforced Wall with Impact Barrier: Design Development and Construction Approach, CDOT Report No. 2018-11, 2018.
- [7] Scott RF, Principles of Soil Mechanics, Addison-Wesley Publ. Co., 1963.
- [8] LS-DYNA user's manual, Vol. III, Version 960, Livermore Softw. Tech. Corp., March 2001.
- [9] DiMaggio, F.L. and Sandler, I.S. Material model for granular soils. J. Eng. Mech. Div., 1971, 97(3): 935-950
- [10] Hallquist, J.O. LS-DYNA Keyword User's Manual (971 R6.0.0)[M]. Livermore:Livermore Software Technology Corporation, 2012.
- [11] Amoco Geotextile ProPex 2044 Specs, Amoco Fabrics and Fibers Company, Austell, GA 30168
- [12] Lu, N., and W. J. Likos. 2004. Unsaturated soil mechanics. New York, Wiley.
- [13] Silvestri-Dobrovolny, C., Schulz, N, Moran, S, Skinner, T, Bligh, R. and Williams, W. MASH equivalency of NCHRP Report 350-approved bridge railings, Project No. 20-07 / Task 395, TTI Project 607141 final report, 2017.
- [14] Sheikh NM, Bligh RP and Menges WL, Determination of Minimum Height and Lateral Design Load for MASH Test Level-4 Bridge Rails, FHWA/TX test report 12/9-1002-5, 2011.
- [15] Sheikh NM, Bligh RP, Menges WL, Schroeder W, Griffith BL and Kuhn DL, Development and Evaluation of MASH TL-4 Guardrail System, FHWA/TX-21/0-7019-R1.
- [16] Dawid Bruski1, Stanisław Burzyński1, Jacek Chróścielewski1, Łukasz Pachocki1 and Wojciech Witkowski1 (2019), On the validation of the LS-DYNA Geo Metro numerical model, MATEC Web of Conferences 262, 10001, 2019 (<https://doi.org/10.1051/mateconf/201926210001> KRYNICA 2018)
- [17] National Crash Analysis Center, Crash Simulation Vehicle Models (accessed 10.03.2016)
- [18] Miele, CR, Plaxico CA, Kennedy JC and Simunovic, S, Heavy Vehicle Infrastructure Asset Interaction and Collision, NTRCI, Oak Ridge National Lab report. (<https://www.roadsafellc.com/NCHRP22-24/Literature/Papers/HEAVY%20VEHICLE%20INFRASTRUCTURE.pdf>)
- [19] Methodology for Validation and documentation of vehicle finite element crash models for roadside hardware (thyme.ornl.gov/fhwa/f800webpage/description/description.html)
- [20] <https://www.nhtsa.gov/crash-simulation-vehicle-models> (but has no Geo nor F800)
- [21] Crash Simulation of Large-Number-of-Elements Car Model by LS-DYNA on Highly Parallel Computers, 2008 (<https://www.fujitsu.com/global/documents/about/resources/publications/fstj/archives/vol44-4/paper09.pdf>)

- [22] Robust Project, WP5-Computational Mechanics Geo-Metro Finite Element model (GM_R3): Improvements of Steering System and Suspensions, I, (2005)
- [23] Nassiopoulos E and Njuguna J, Finite element dynamic simulation of whole rallying car structure: Towards better understanding of structural dynamics during side impacts, 8th European LS-DYNA Users Conference, Strasbourg, May 2011.
- [24] Ray MH, Mongiardini, Atahan AO, Plaxico CA, and Anghileri M, Recommended Procedures for Verification and Validation of Computer Simulations used for Roadside Safety Applications, NCHRP Project 22-24 Interim report, 2008 (https://www.roadsafellc.com/NCHRP22-24/Interim_Report/Old_revisions/RevisedInterimReport.pdf)
- [25] American Association of State Highway and Transportation Officials. Manual for Assessing Safety Hardware (MASH), AASHTO Subcommittee on Bridges and Structures, Washington, D.C., 2016.
- [26] https://www.csppacific.co.nz/uploads/literature/thrie-beam_technical_data.pdf